5G Microwave vs. Millimeter-wave MIMO Wireless Mobile Systems

Christian Ballesteros Sánchez

A Master's Thesis submitted to the School of the ETSETB in partial fulfillment of the requirements for the degree of

Master in Telecommunication Engineering

Supervisor: Luis Jofre Roca

Universitat Politècnica de Catalunya

July 2018

Abstract

The next generation of wireless systems, 5G, is intended to cover plenty of new emerging applications such as utra-high resolution multimedia systems, industry 4.0, self-driving vehicles and smart cities. All those different applications require a technology able to deal with three main type of scenarios: enhanced Mobile Broadband (eMBB) systems, Ultra-Reliabe and Low Latency Communications (URLLC) and massive Machine-Type Communications (mMTC). The necessity of achieving high-data rates in wireless systems have led to multi-antenna configurations and Multiple Input Multiple Output (MIMO), and massive MIMO, geometries have been essential to improve the global performance.

Otherwise, finding a solution that fits in all cases is challenging and several approaches may be considered according to the initial recommendations from the standardization entities. In this thesis, a system point of view is provided to address the problem, placing an emphasis on the physical analysis of the communications channel. In particular, different solutions are proposed and compared, from the most immediate future approach (at microwave frequencies) to mid- or long-term solutions (in millimeter-wave bands).

Acknowledgement

This entire thesis would not be possible without the priceless contribution of many people that helped in one way or another to the development of the work herein presented. First of all, I want to express my gratitude to Prof. Luis Jofre, who has been my supervisor and has entirely reviewed this work. Every word has been enormously helpful and I am glad to say that there is still a long path to walk together trying to break the frontiers of future antennas and communications.

Special thanks to Andreas Pfadler, my workmate and good friend. We have grown a lot this last year and I wish you every success in the new stage of your career.

It is also mandatory to mention all professors and staff from the laboratory that have helped me in many stages. I really appreciate your work.

Finally, thank you to my family and friends, who always support me. If I have reached my goals, it is just because of you.

Contents

Glossary

3GPP 3rd Generation Partnership Project

AAS Active Antenna Systems

ATIS Alliance for Telecommunications Industry Solutions

BS Base Station

DSRC Dedicated Short Range Communications

ECC Electronic Communications Committee

EDGE Enhanced Data rates for GSM Evolution

eMBB enhanced Mobile Broadband

eNB Evolved Node B

ETSI European Telecommunications Standards Institute

FCC Federal Communications Commision

GEO Geosynchronous Equatorial Orbit

gNB Next Generation Node B

GO Geometrical Optics

GPRS General Packet Radio Service

GSM Global System for Mobile communications

GTD Geometrical Theory of Diffraction

IMT International Mobile Telecommunications

ISM Industrial, Scientific and Medical

ITS Intelligent Transportation Systems

ITU International Telecommunication Union

LEO Low Earth Orbit

LOS Line of Sight

LTE Long Term Evolution

MIMO Multiple Input Multiple Output

MLFMM Multilevel Fast Multipole Method

mMTC massive Machine-Type Communications

mmWave millimeter-wave

MoM Method of Moments

NLOS Non Line of Sight

NR New Radio

NSA Non-Standalone

OFDMA Orthogonal Frequency-Division Multiple Access

PCB Printed Circuit Board

PEC Perfect Electric Conductor

PO Physical Optics

RAN Radio Access Network

RL Return Loss

SA Standalone

SDR Software Defined Radio

SISO Single Input Single Output

SNR Signal to Noise Ratio

TEM Transverse electromagnetic

UMTS Universal Mobile Telecommunications System

URLLC Ultra-Reliabe and Low Latency Communications

UWB Ultra-wideband

V2I Vehicle-to-Device

V2I Vehicle-to-Infrastructure

V2I Vehicle-to-Network

V2I Vehicle-to-Pedestrian

V2V Vehicle-to-Vehicle

V2X Vehicle-to-Everything

VNA Vector Network Analyzer

VSWR Voltage Standing Wave Ratio

List of Figures

List of Tables

Chapter 1

Introduction

The work presented in this thesis intends to describe a system-level study of the next generation of cellular communications, i.e., 5G. The focus is mainly put on the impact of new multi-antenna geometries at different operating bands, including microwave and millimeter-wave (mmWave). A deep analysis is carried out, from the description to the simulation and measurement of realistic channels.

Initially, the benefits of such type of systems have to be detailed, specially emphasizing the differences in terms of performance at each of the bands of interest. The study covers regular MIMO geometries, which were already introduced in past generations, and massive MIMO, allowing the implementation of new beamforming techniques.

Due to the variety of bands that must be analyzed, a "general purpose" antenna is designed. It allows to reuse the same antenna geometries regardless the operating frequency, which may vary from the S-band to the first mmWave frequencies. Then, by means of Software Defined Radio (SDR) devices, a test campaign is carried out to evaluate the channel performance and compare the results with initial analytical models. These measurements are performed both at microwave and mmWave bands, which allows a comparison of the available frequencies in terms of capacity and MIMO gain.

1.1 Motivation

The new emerging applications in modern communication systems include a wide range of requirements, such as faster data rates, lower latency and very large networks. The necessity of fitting all of them in a single technology is a challenge at all levels. In particular, this thesis contributes with some proposals on MIMO systems and a physical-level analysis of them.

The importance of (massive) MIMO geometries is already proven, but more detailed investigations are required to fully understand the performance of this new technological wave. One of the main driving forces is the automotive industry, which moves towards electric, connected and autonomous devices that must be considered in the new technological era. After some previous studies in the field of vehicle communications

[1,2], the scope is extended to a more general scenario and empirical measurements are introduced to validate physical models.

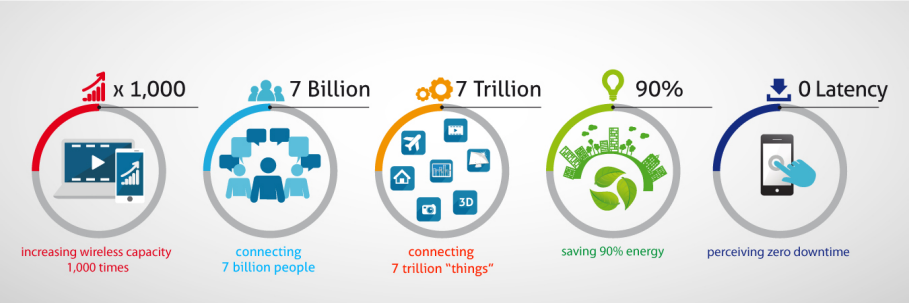

Figure 1.1: Goals of 5G-PPP [3].

In the context of next-generation communications, the 2020 horizon [4] is pushing the industry and research entities to move fast towards the development of faster, more efficient and flexible technologies in wireless communications. Over the last years, regulation bodies have defined some initial requirements as a starting point but specific solutions are still under investigation. The goals are very heterogeneous and there is also the necessity of combining different radio access technologies (interoperability) such as LTE or Wi-Fi with new microwave or mmWave networks. Therefore, a wide range of solutions is under discussion, but this thesis is mainly focused on the physical evolution of upcoming 5G networks that will imply a complete change in our understanding of the radio channel.

1.2 A Brief Look to History

This section is devoted to a description of the currently available technologies for mobile communications, emphasizing the improvements introduced at each new era, the expected changes with regard to the next generation, and a historical view of an important novelty which will be introduced in future networks: the mmWave band.

1.2.1 Evolution of Mobile Communications

Mobile communications have evolved significantly over the years. After some initial approaches based on the analog voice service (first generation, 1G), Global System for Mobile communications (GSM) was introduced in the 1990s as the first global cellular system. The enormous popularity and great performance in digital voice transmission have made it the most used standard until recent years, reaching more than 6 billion subscribers in 2013 [5]. The use of time multiplexing instead of (only) frequency channelization made possible to successfully allocate more users.

2G systems also introduced short messaging and low-speed data transmission with General Packet Radio Service (GPRS) and Enhanced Data rates for GSM Evolution (EDGE) evolutions but the explosion of Internet created the necessity of higher speeds

for packet switching networks. In consequence, the third generation (3G) of mobile communications was born under the Universal Mobile Telecommunications System (UMTS) standard. A new architecture was introduced mainly focused on faster Internet connections. Basically, the GSM/GPRS structure devoted to voice was preserved, whereas new elements were introduced to achieve higher data rates by means of code multiplexing, wider channel bandwidths and more robust and faster Radio Access Networks (RANs).

	1G	2G	3G	4G	5G
Deployment	1980s	1990s	2003	2009	2020?
Multiplexing	FDMA	TDMA	CDMA	OFDMA	OFDMA
Services	Analog mobile telephony	Digital voice and short messaging	Mobile Internet	IP Telephony, high-speed Internet access	Ultra-high-speed Internet, IoT, autonomous vehicles
Evolutions	–	GPRS, EDGE, EGPRS	HSPA, HSPA+	E-UTRA, LTE Advanced, LTE Advanced Pro	–
Max. Rate	Analog voice only	<500 kbps	84 Mbps	1 Gbps	100 Gbps

Figure 1.2: Comparison between cellular network generations.

The increasing number of connected devices seemed to be unstoppable and new applications such as multimedia streaming and social networks required even larger speeds. In addition, packet switching was seen as the most efficient implementation and IP telephony started to substitute conventional digital voice. All those requirements were covered by the fourth generation (4G), which was progressively implemented throughout the second decade of the 21st century. The most significant change was the multiple-access method: Orthogonal Frequency-Division Multiple Access (OFDMA). It is also the chosen method for the future generation, since orthogonal carriers provide really good performance in burst transmissions with higher spectral efficiency compared to spread spectrum multiplexing [6].

Larger bandwidths and multi-antenna geometries have been also introduced to achieve even higher speeds. These two improvements will become more relevant regarding next-generation communications in 5G. Future networks must cover a wide variety of applications in completely different situations. Figure 1.3 shows the most relevant cases, which can be classified in three main types, depending on the specific requirements:

- **Enhanced Mobile Broadband (eMBB) communications**. They are characterized by a very high data rate demand, specially for downlink connection. They include any high resolution multimedia streaming application and large size file transfers, which are the two main driving forces in user entertainment. Capacity is the main goal, as it defines the achievable rate of a communication channel.
- **Ultra-Reliabe and Low Latency Communications (URLLC)**. Time delay and latency are the relevant parameters in this case. The most representative use cases are self-driving cars, eHealth applications and real-time multimedia, such as cloud gaming. Packet size is not as important as the travelling time from one side to the other and it becomes particularly critical regarding safety applications.

- **Massive Machine-Type Communications (mMTC)**. The increasing number of connected devices is leading cellular communications to a new paradigm when thinking of network management. Connected houses, smart cities, car communications, smart grids and many other applications imply the inclusion of a massive number of new devices in the network. The aggregated traffic requires an enhancement in backhaul links but also an improved radio access network to manage all those devices properly.

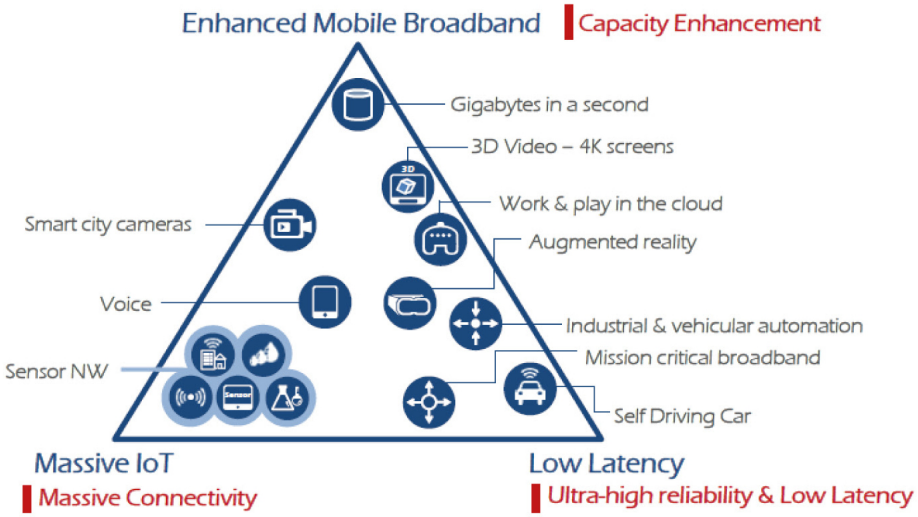

Figure 1.3: Triangle of 5G applications [7].

All those emerging applications are driving communications to a more complex scenario and many stakeholders have to agree on solutions to address the new demands. It is impossible to fit all them in a single closed technology and, in consequence, 5G is thought as a collection of different technologies (with some common elements) that try to fit in each use case.

For instance, initial approaches are concentrated on sub-6 GHz microwave bands. They try to reuse as much as possible existing facilities and adapt them to next generation networks, i.e., Non-Standalone (NSA). The next step consists in moving to an independently operating network, introducing new bands at higher frequencies, up to mmWave, and it will conclude the migration to the new cellular generation. More details about existing standards and their evolution are provided in section 2.1.

The use of higher frequencies will allow manufacturers the introduction of multi-antenna geometries with larger amount of elements in less space. This new type of structures make massive MIMO a feasible solution. Then, beamforming techniques may be used to improve system performance and efficiency. A preliminary analysis about the use of this new geometries in Vehicle-to-Infrastructure (V2I) scenarios was also detailed in [1] by the author and this research group.

Massive geometries are an state-of-the-art hot topic nowadays, but they does not seem to be part of first 5G releases, even though many solutions are being investigated and some initial experiments have been already carried out [8–10]. In this work, massive

antennas are not a central topic either, but advanced MIMO structures are analyzed.

1.2.2 125 Years of mmWave Research

Since mmWave band is a promising candidate to allocate the new generation of mobile communications and many other applications (such as radar tomography or the already existing body scanners), it may seem a newfound type of wireless of communications. On the contrary, recent innovations are the consequence of many years of research. Moreover, one of the first experiments in wireless communications was performed at a frequency of 60 GHz at the end of the 19^{th} century.

In November 1894, an Indian scientist named Jagadish Chandra Bose performed the first demonstration of wireless transmission [11, 12]. In the experiment, Bose remotely fired a gun and rang a bell by means of electromagnetic waves and very primitive instruments, as shown in Figure 1.4. He used horn antennas, a Galena detector and other devices, such as an open resonator or a spiral spring coherer (both developed by himself). Despite the available resources and the lack of knowledge in this field at that time, Bose was able to successfully perform his experiment, transmitting the 60 GHz signals through two walls and a distance between both ends of 23 m. This revolutionary experiment was the spark for the subsequent discoveries and investigations in the field of wireless communications. It is for that reason that, more than 80 years late, Sir Neville Mott, who won the Nobel prize in 1977 thanks to his investigation in solid state electronics, said that "J.C. Bose was at least sixty years ahead of his time... In fact, he had anticipated the existence of P-type and N-type semiconductors"[11], stressing his invention of Galena crystals, which were used as a receivers up to ultraviolet frequencies.

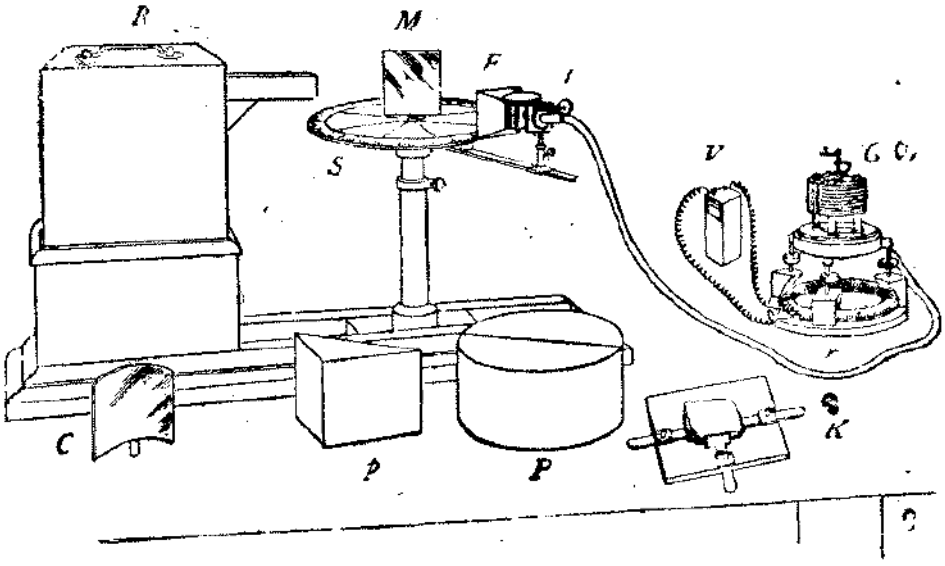

R, radiator ; S, spectrometer-circle ; M, plane mirror ; C, cylindrical mirror ; *p*, totally reflecting prism ; P, semi-cylinders ; K, crystal-holder ; F, collecting funnel attached to the spiral spring receiver ; *t*, tangent screw, by which the receiver is rotated ; V, voltaic cell ; *r*, circular rheostat ; G, galvanometer.

Figure 1.4: Instruments used by J.C. Bose during his investigations [13].

Furthermore, much longer wavelengths were mainly used in latter experiments until the second half of the 20^{th} century. At the beginning, many investigations were centered in the characterization of materials and electromagnetic waves, like the studies of E. F. Nichols and J. D. Tear in 1923 [14,15] or C. E. Cleeton and N. H. Williams in 1934 [16]. The next step forward after Bose's discoveries regarding mmWave communications was in the 1950s, with the invention of the maser by the Nobel prize in Physics Charles Hard Townes. This device was the predecessor of the laser and it was based on the photonic radiation of ammonia mollecules. Due to the low energetic gap, the frequency of emission was 24 GHz.

During next decades, the amount of research in millimetric bands did not suffer the expected impulse. The U.S. Army put a lot of efforts into the development of high resolution radars in the band of 70 GHz, but the emergence of the laser put the focus on optical bands in the field of communications. Even so, the evolution of satellite communications and the rivalry between USA and the Sovietic Union to lead the race to space drove the Americans to create many remote sensing satellites carrying radiometers in the mmWave band, like the ATS-E [17] in the 1960s (see the equipment in Figure 1.5) or Nimbus-F [18] in the 1970s.

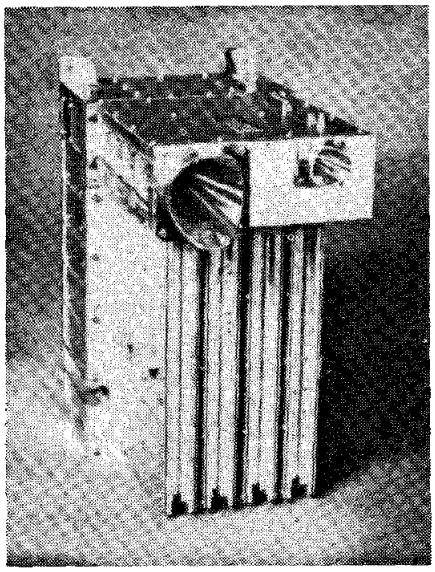

Figure 1.5: ATS-E millimeter-wave transmitter [19].

Up until now, mmWave communications have been mainly devoted to radiometry and radar, but the interest in those bands is *in crescendo* for a wide variety of applications. The necessity of more spectrum to allocate new technologies, with larger bandwidths, makes this region appropriate for 5G systems. New challenges will come up but a huge community of researchers and engineers is working to overcome them and provide feasible and innovative solutions.

In 2020, the horizon for next generation of mobile communications will coincide with the 125^{th} anniversary of Bose's experimental demonstration in the Town Hall at Calcutta. The inclusion of modern mmWave technologies in the upcoming systems, that descend from his initial discoveries, is the greatest tribute to his figure.

1.3 Communications at mmWave Bands

The demanding applications of future 5G networks entail the necessity of finding innovative solutions far from the crowded spectrum below 6 GHz to reach values of bandwidth around few GHz. Some systems, specially in the automotive field, also require low latency communications and high accuracy target detection. All these requirements have motivated engineers to move up in frequency and mmWave band is the next frontier for regulators and industry.

The use of millimetric bands represents a challenge from many points of view, but it is an almost unexplored region of the spectrum for mobile communications, which could benefit from other aspects. The most important strength is the available bandwidth. It needs to be regulated first in order to allocate all requesting candidates but, once the spectrum is divided, an enormous potential can be exploited to establish ultra-fast and massive links. It is still far from very energetic frequencies, so it is harmless and suitable for other applications such as tomography [20, 21] and radar imaging [22, 23].

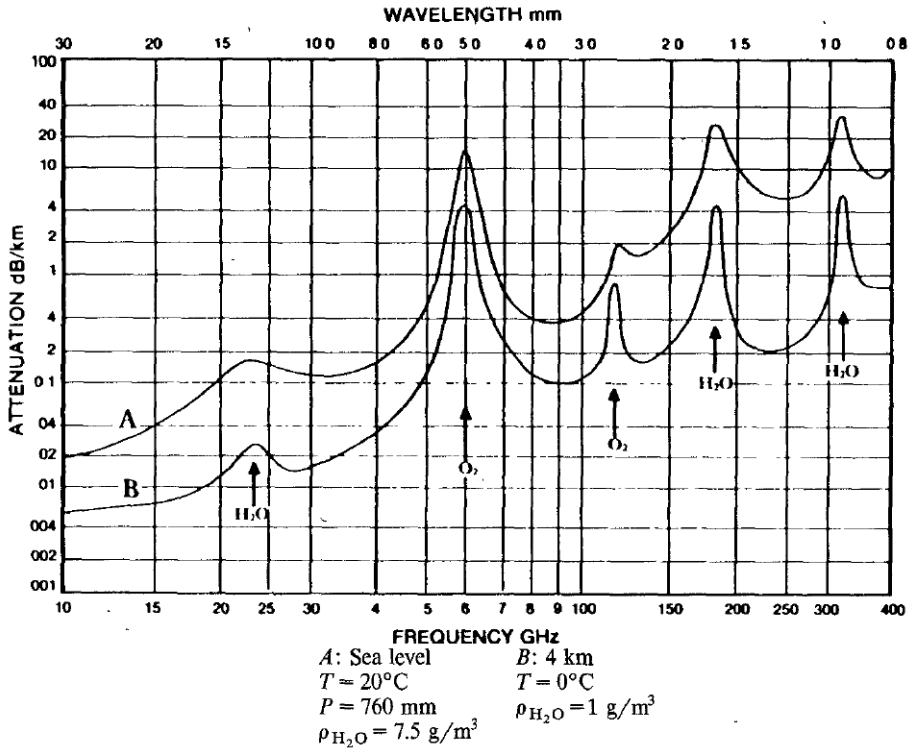

Figure 1.6: Average atmospheric attenuation of millimeter waves [24].

On the other hand, the most limiting factor is attenuation. Figure 1.6 shows the attenuation of electromagnetic waves in the range between 10 and 400 GHz and its relation with atmospheric gases. Many peaks can be observed due to the content of oxygen and water vapor. At the particular frequency of 60 GHz, oxygen molecules present a resonance that absorbs a great amount of energy, making communications unfeasible for long distances. In addition, the free-space Friis transmission equation defines a direct relation between frequency and path loss [25] and penetration in buildings and other objects is also considerably reduced, so direct view from the transmitter

to the receiver is usually a must. All together leads to small cells and reduced distance systems if a feasible communication is wanted. Different coverage regions can be defined according to the technology, and frequency, used in each case. Then, hierarchical cell structures seem to be the logic behind future mobile networks.

1.4 Objectives

The main goal of this thesis is to provide tools and techniques to better understand and evaluate communications at future 5G frequency bands, both microwave and mmWave. In particular, channel characterization is emphasized to analyze the performance of mobile systems at a physical level.

The work here described can be structured according to the following statements:

- Investigate the current state of next-generation networks and determine band allocation according to different applications and standards.
- Design of a multi-antenna system to test MIMO communications, capable to cover the widest range possible according to the previously found requirements.
- Definition of valid figures of merit in order to evaluate physical effects and system performance.
- Simulation of a realistic indoor and outdoor environment to provide initial knowledge about the channel behavior.
- Measure and compare real channels with simulations to validate the models and experimentally evaluate the benefits of multi-antenna geometries and their impact on the radio channel. While to approach intends to be quite general, a certain emphasis has been devoted to mobile systems.

1.4.1 Work Plan

The project is divided in three main parts:

- The design and manufacturing of an Ultra-wideband (UWB) antenna
- The simulation and testing campaign of an indoor MIMO system
- The simulation of a V2I communication environment

In addition, documentation and writing tasks must be carried out as well as the preparation of the final presentation. The following simplified Gantt diagram summarizes in the time domain the main working areas.


2018
Jan
Feb
Mar
Apr
May
Jun
Jul
Documentation
UWB Antenna
EuMW Paper Submission
Indoor MIMO System
V2I Simulations
Writing
TFM Report
Presentation
TFM Presentation

Table 1.1 indicates with more detail the individual tasks for each group.

Table 1.1: Project tasks and milestones.

Objective	Task	Start	End
Documentation		**19-feb**	**30-mar**
	Mobile comms	19-feb	02-mar
	mmWave	05-mar	16-mar
	Standards & Regulation	19-mar	30-mar
UWB Antenna		**29-ene**	**23-mar**
	Design	29-ene	31-ene
	Optimization	01-feb	07-feb
	EUMW'18 paper writing	05-feb	12-feb
	Final simulations	08-feb	09-feb
EUMW'18 paper submission		**12-feb**	
	Single manufacturing	13-feb	16-feb
	Single testing	19-feb	20-feb
	Re-optimizing for manufacturing	21-feb	02-mar
	MIMO manufacturing	05-mar	16-mar
	Ground plane	05-mar	23-mar
EuCAP'18		**12-mar**	**13-abr**
	Poster preparation	12-mar	16-mar
	Printing service	19-mar	23-mar
	Conference	09-abr	13-abr
Indoor MIMO System		**02-abr**	**17-jul**
	End-to-end design	02-abr	06-abr
	Creation of scenario	16-abr	27-abr
	Pattern and Propagation Simulations	30-abr	11-may
	Analysis of simulation results	14-may	18-may
	Improved simulations	21-may	25-may
	Research of SDR solutions	28-may	01-jun
	Initial SDR tests	04-jun	15-jun
	VNA sounder design	18-jun	22-jun
	Buy cables and connectors	25-jun	11-jul
	Horn antennas design	02-jul	06-jul
	Testing campaign	12-jul	12-jul
	Analysis of measurement results	13-jul	16-jul
V2I Simulations		**04-jun**	**06-jul**
	Definition of geometries	04-jun	08-jun
	Simulation of mmWave antennas on car	11-jun	15-jun
	Propagation simulation at 26 GHz	28-may	29-may
	Multi-antenna postprocessing	18-jun	29-jun
	Export and analysis of results	02-jul	06-jul
Writing thesis report		**02-abr**	**17-jul**
	Introduction & State of Art	02-abr	27-abr
	UWB antenna	30-abr	25-may
	Indoor MIMO	28-may	17-jul
	V2I Communications	18-jun	13-jul

Table 1.1: (continued)

	Conclusions	16-jul	17-jul
	Initial Revision	09-jul	13-jul
	Final Version	16-jul	17-jul
TFM report delivery		**17-jul**	
Preparing presentation		**17-jul**	**23-jul**
TFM presentation		**24-jul**	

Chapter 2

The Revolution of Next-Generation Communications

5G is rising over the horizon, initially expected to lean on in 2020, and several agents are joining efforts to increase the pace in order to meet the target specifications. The explosion of some features previously introduced in 4G such as carrier aggregation and spatial multiplexing and other new technological advances like Active Antenna Systems (AAS) (beamforming and beam steering) are a big challenge that must be properly driven as we approach to next-generation mobile systems. It implies the allocation of new frequency bands to achieve the desired requirements and find proper solutions far from the overcrowded regions of the spectrum.

In the context of future mobile networks, car communications is maybe the most challenging field. Extremely low latency and a massive number of potential users lead to the necessity of finding smart and reliable solutions in short term, since Intelligent Transportation Systems (ITS) are an upcoming reality. A section devoted to connected cars emphasizes the importance of research in this direction and provides the initial guidelines to include them as part of the next-generation network.

2.1 Regulatory Bodies and Standards

Standardization entities have been defining the pathway to provide a solid base to all researchers and companies. From their recommendations, the most important features can be extracted to form a criterion to develop the upcoming technologies. Despite there is still a long way off before stating that 5G is a reality, the first stages of the development process are already in motion. The future of International Mobile Telecommunications (IMT) is closer than it seems.

The global regulator of spectrum is the International Telecommunication Union (ITU), from the United Nations. Every organization must design its own standards according to the specifications defined by the former. IMT-2020 final details are ex-

pected to be released in WRC-19, but industry needs to start developing new products in advance. Nowadays, ITU has already allocated many bands for mobile applications at low frequencies (below 6 GHz, see Table 2.1). Some of them are already in use, but others offer a potential allocation for low- and mid-frequency 5G.

Table 2.1: Sub-6 GHz IMT bands [26].

IMT bands
450–470 MHz
698–960 MHz
1427–1518 MHz
1710–2025 MHz
2110–2200 MHz
2300–2400 MHz
2500–2690 MHz
3300–3400 MHz
3400–3600 MHz
3600–3700 MHz
4800–4990 MHz

As in any wireless system, there is a trade-off that must be considered between coverage and speed (throughput). Lower bands can operate over a wider area but bandwidth is quite constraint. In order to provide a soft transition to the new generation, as well as macro-cell coverage, are already working with bands below 6 GHz. They vary according to each country, but they are basically around 700 MHz, 1500 MHz, 3600 MHz and 4400 MHz. In particular, Europe chose as pioneer 5G band the allocation at 3400–3800 GHz [27].

One of the greatest revolutions in 5G networks will be the use of mmWave frequencies. In the last WRC-15, the ITU already defined some candidate bands and the national regulatory bodies have chosen a preliminary allocation. This is a summary of high-frequency bands by country:

- In Europe, the 24.25–27.5 GHz band is chosen, following the ITU recommendations, but 31.8–33.4 GHz and 40.5–43.5 GHz are reserved as candidates as well.
- The Federal Communications Commision (FCC) in the USA has allocated two bands between 27.5–28.35 GHz and 37–40 GHz.
- South Korea tested a prototype of 5G communication in the 2018 Winter Olympics in the 27.5–28.35 GHz and pretends to include also 37.5–40 GHz.
- Japan is preparing the initial 5G release in 2020 between 27.5–29.5 GHz.
- China maximizes compatibility allocating both 24.25–27.5 and 27.5–29.5 GHz.

In brief, 5G communications are to be carried out mainly in three regions of spectrum: below 1 GHz for longer ranges and massive devices, at 3.4–3.8 GHz providing wider bandwidths and at 24–29 GHz if even larger bandwidths are required; though other bands may be additionally used in some particular countries.

The 3rd Generation Partnership Project (3GPP), which comprises different organizations including the European Telecommunications Standards Institute (ETSI) from Europe or the Alliance for Telecommunications Industry Solutions (ATIS) from the USA, is responsible for the development of the new standards regarding mobile communications, as in the case of the third and fourth generations. Figure 2.1 shows the expected quarterly timeline for the upcoming Release 15. A first set of specifications was approved at the end of 2017 for the NSA version. It tries to integrate new elements to the existing 4G network in order to move smoothly to the next generation. By the end of 2018, 5G Phase 1 will be finished including the Standalone (SA) initial specifications and Release 15 will be completed.

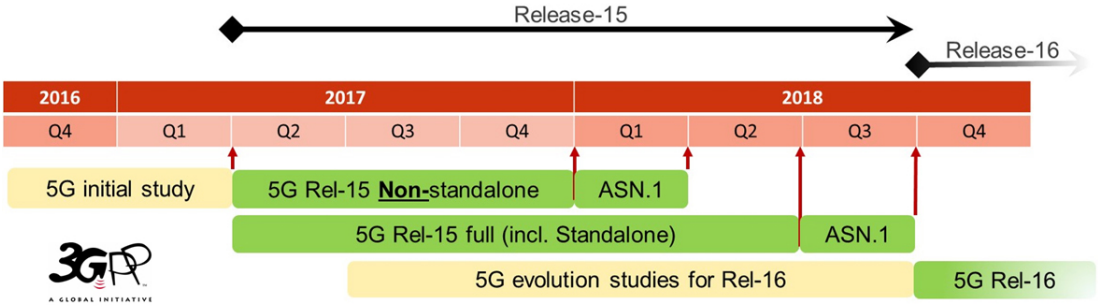

Figure 2.1: Timeline of 3GPP Release 15 [28].

Parallel to 5G, Long Term Evolution (LTE) Advance Pro is evolving as an early-stage, known as 4.9G. Since 4G is alive and still growing, the NSA version becomes critical to take advantage of the previous generation as much as possible when constructing new architectures. Figure 2.2 depicts different architectures regarding the RAN configuration, moving from an initial design in which the Next Generation Node B (gNB) acts as slave towards the parallel operation together with the Evolved Node B (eNB). This architecture options were approved in the 3GPP RAN Meeting at the end of 2017 and new specifications are expected to be introduced over next months.

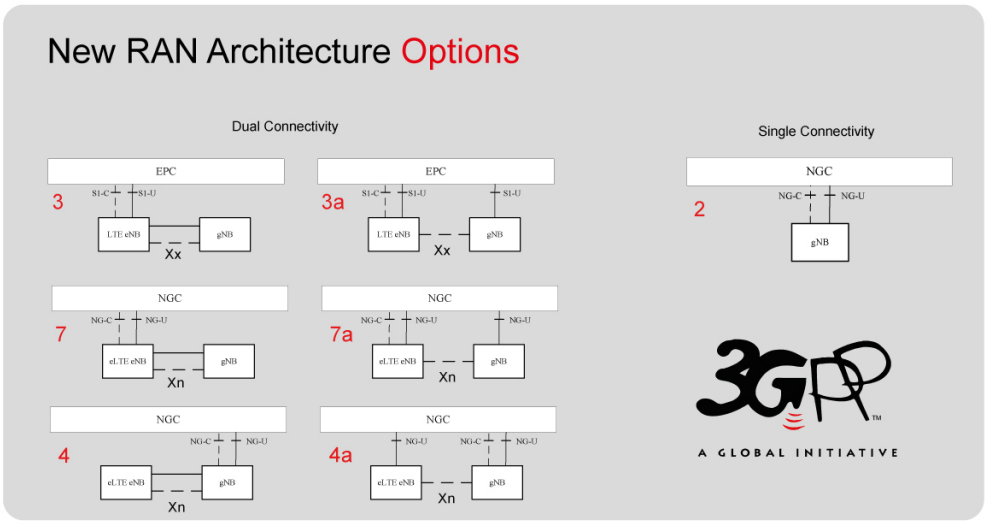

Figure 2.2: New RAN architecture options [29].

The new air interface under development for the next generation, called 5G New Radio (NR), represents a significant change in the understanding of wireless communications. Scalability and efficiency come up as two key factors stronger than ever. This is the reason why (hybrid) beamforming and network flexibility appear in the horizon. The use of beamforming base stations allows achieving higher data rates, less inter-cell interference and better efficiency, not only to the final user but also between base stations using a mmWave backbone. On the other hand, higher frequency (required to obtain narrow enough beams) reduces the coverage and cells may be categorized according to the final application or the reachable distance to the user. Network widespread growth and new capacity requirements lead mobile communications to the use of small cells and the variety of frequencies introduced in 5G allows the creation of hierarchical networks. For example, a small base station can act as a relay between two cars which are not able to communicate directly around a corner or specific cells can be created for large scale events (e.g., a football match) with enough bandwidth to provide service to thousands of users in a small area.

The last issue regulators and manufacturers must deal with is multiconnectivity. The future of wireless communications is not seen as a set of independent networks but as a more complex structure where all devices will be able to connect to each other without taking into account which is their access technology.

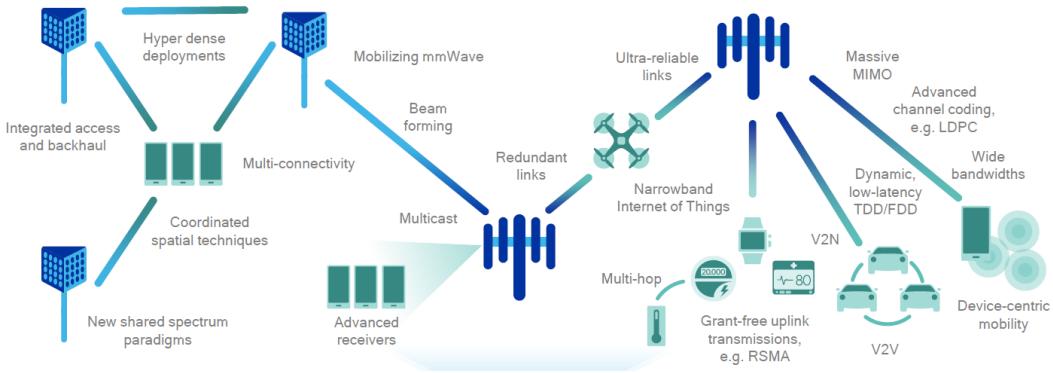

Figure 2.3: Example of 5G network [30].

Regarding the mmWave spectrum, not only mobile 5G networks are expected to be allocated at those frequencies. They will have to coexist with other applications [31]:

- **WiFi Gigabit (802.11ac)**. It is an evolution from the previous 802.11n that pretends to use the unlicensed band in the 57–63 GHz region. 802.11ad tries to reach ultra-high-speed WiFi connection (up to 4.6 Gbps) with a large number of antennas and improved bandwidth in the mmWave region.
- **Satellite broadband communications**. Data transmission from/to Low Earth Orbit (LEO) and Geosynchronous Equatorial Orbit (GEO) satellites is moving towards higher frequencies as well. Some portions of the spectrum in the Ka band, between 26 and 40 GHz, are devoted to this kind of systems.
- **Automotive radar**. Security and self-driving applications tightly rely on radar systems. Despite the use of optical cameras, they suffer from visual blockage if

there are obstacles in between the target and the user. New car radar devices are operating at 24 GHz and in the 77–81 GHz band.

- **Wireless backhaul**. The FCC reserved bands at 71–76, 81–86 GHz and 92–95 GHz for high-density fixed wireless services, in order to reduce wired connections and make use of new techniques such as beamforming to improve point-to-point radio links.
- Many **unlicensed bands** can be also found at mmWave frequencies that could be exploited. Some Industrial, Scientific and Medical (ISM) bands are at 24–24.25, 61–61.5, 122-123 and 244–246 GHz.

2.2 Connected Cars in a Connected World

Every day there is a growing necessity of globally connecting things surrounding us, and cars are not an exception. Furthermore, vehicle communications are one of the most challenging and promising fields with respect to next-generation networks. Their introduction into mobile systems as a new type of user, with their very particular requirements, implies a reorganization of communications from what we already know.

There is a wide range of applications and benefits that can be obtained by means of adding communication capabilities to vehicles: roads can be safer since driving will not exclusively rely on the driver, who will be assisted at any moment, traffic flow can become more efficient, self-driven vehicles can be massively introduced if they have a robust and fast connection between them (and to other elements, such as pedestrians) and, in consequence, multimedia and many other services can be delivered to the passengers.

According to the specific situation, vehicle communications are classified as:

- **Vehicle-to-Vehicle (V2V)**. Two or more vehicles communicate between them for route prediction, collision avoidance or platooning. Very low latency is required, since speed is much higher than regular mobile users.
- **Vehicle-to-Infrastructure (V2I)**. Traffic signalling and relaying (e.g., if no direct communication is possible between users) are the main use cases.
- **Vehicle-to-Pedestrian (V2I)**. Vehicles can also be connected to pedestrians and bicyclist to track them and make their route safer.
- **Vehicle-to-Device (V2I)**. This type includes any kind of data exchange with any other device, inside or outside the vehicle.
- **Vehicle-to-Network (V2I)**. The vehicle is directly connected to the cellular (Internet) network. The most important applications are cloud services and real-time traffic management.

In general terms, Vehicle-to-Everything (V2X) systems are expected to be allocated in two main bands, depending on the technology underneath [32, 33]. First, the Electronic Communications Committee (ECC) issued a recommendation regarding ITS to

use the 5.9 GHz band for this purpose, with 70 MHz total bandwidth, as can be seen in Figure 2.4.

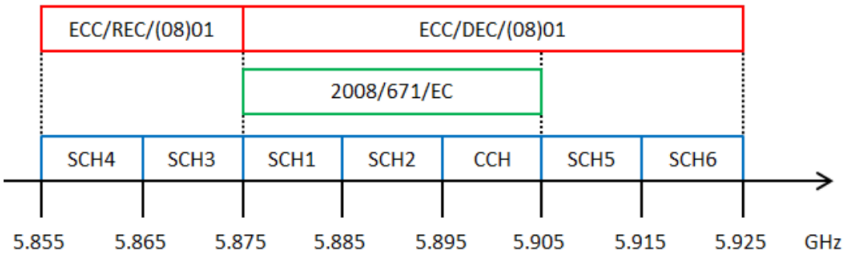

Figure 2.4: V2X in the 5.9 GHz band [32].

This band has been adopted by ETSI to deploy the ITS-G5 technology [34], which is globally known as IEEE 802.11p [35]. It is pretended to be used for the V2V and V2I cases, allowing a fast and ultra-low latency connection between cars. They correspond to the also known as Dedicated Short Range Communications (DSRC).

The mobile industry is also involved in the development of new technologies for vehicle applications. Release 14 of 3GPP specifications already defined two modes of operation for V2V communications: Mode 3 (cellular-assisted V2V)and Mode 4(pure ad-hoc V2V). They are planned to work at the 5.9 GHz unlicensed region of the spectrum and it implies that this band must be properly shared with ITS-G5.

On the other hand, car and antenna manufacturers want to take advantage of better propagation properties of lower frequencies, specially in the case of Non Line of Sight (NLOS) links. It must be also considered that antennas will be larger if same efficiency is wanted.

In the case of LTE-V2X, it specifies a redundant communication channel in the 3.4–3.8 GHz band. It is specially useful in case of critical applications such as platooning, providing more robust and safer connections.

Figure 2.5 depicts a summary of the main V2X technologies.

Technology	Region	Standard
802.11p	US	IEEE 802.11-2012, IEEE 1609.2 - .4, SAE J2735 and SAE J2945/x series
802.11p	Europe	"ITS-G5", ETSI ITS series
802.11p	Japan	ARIB STD-109
Cellular LTE	Global	3GPP TS 22.185, TS 23.285 for V2X and LTE, and TS 36 series for radio access
Cellular 5G	Global	3GPP TS 22.186; TS 23.501 for network architecture 3GPP 38 series for the radio access

Figure 2.5: V2X technologies by region [33].

Chapter 3

UWB Antenna Design

The wide range of frequencies that need to be analyzed takes to only two types of solutions: a specific antenna design for each band of interest or an ultra-wide band design in order to cover the widest range possible and reuse the same geometry in all cases. Device manufacturers prefer to reduce the number of antennas to easily integrate them in their designs. A common practice is to use notched-band wideband antennas, as in [36], which are implemented to work in many bands, but they do not cover the entire usable spectrum. They are useful when particular bands want to be used and they highly avoid the out-of-band interference and noise effects.

In the specific case of this work, the goal is to design and implement an antenna covering from the lowest S band frequencies up to mmWave Ka band. It may fit in any sub-6 GHz application (and above 2 GHz) and it could be used to test the 24.25–27.5 GHz European 5G band. The operational bandwidth is not restricted either and it allows fully frequency reconfiguration within the specified range. The latter is specially useful when SDR is used. Testing and prototyping is then much easier, despite the design could be optimized for the final integration within a commercial platform.

3.1 The Wideband Monopole

According to the FCC [37], "any device where the fractional bandwidth is greater than 0.25 or occupies 1.5 GHz or more of spectrum" can be considered to be UWB. In the case of study, the goal is even more ambitious and the geometry must be properly designed to operate at a very large range of frequencies, from a circuit point of view (matching) and regarding the electromagnetic radiation (fields distribution). Then, not only the antenna impedance has to be considered during in the design, but the radiation pattern too. In general, antennas in mobile communications must be able to radiate to any direction in space.

On the other hand, the size must be small enough to include it in a preliminary prototype system, even it could be further optimized for a final implementation. Even though the antenna dimensions are not a critical constrain, it must be considered in the design. As one of the potential use cases is vehicle communications, it should fit in

a shark-fin radome, typically used on car-roof antennas.

These are the main requirements that the antenna has to fulfill:

- The Voltage Standing Wave Ratio (VSWR) is equal or smaller than 2 for the bands of interest, 2.4–2.7 GHz, 3.4–3.8 GHz, 5.8–6 GHz, and 24.25–27.5 GHz. It corresponds to Return Loss (RL) greater than 9.54 dB, or S11 smaller than −9.54 dB.
- The maximum radius of an sphere enclosing the antenna should be smaller than 2 cm. It allows the antenna to be small enough to fit into a shark fin-like radome, typical in the automotive industry.
- The input impedance phase shift over the frequency must be linear to reduce dispersion [38].
- Gain variations over the horizontal plane must be smaller than ±10 dB for all bands of interest. It ensures an almost omnidirectional radiation, preventing deep nulls in the pattern.

Given the previous requirements, the chosen geometry is a monopole. It provides an omnidirectional radiation on the horizontal plane and its inclusion on a car is not as challenging as other more complex structures. In this case, the UWB version of a monopole has to be considered, as they are essentially narrowband.

In order to enlarge the operating range of frequencies, the geometry is transformed to a conical radiator. The great UWB performance of this type of antennas has already been proven in [39,40]. Due to the physical contraints of the radome, which may include several antennas as explained in Section 3.5, the cone is not following a symmetry of revolution over the vertical axis. The two dimensions over the horizontal plane are optimized separately, ending up in an elliptical base.

Additionally, an hemiellipsoidal dome is included on top of the inverted cone, as shown in Figure 3.1. It enlarges the superficial length from the feeding point to the top, providing lower frequency resonance without a proportional increase in height.

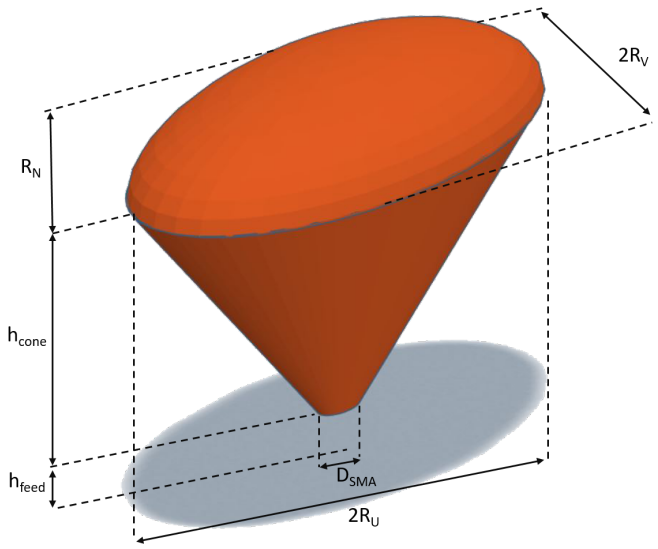

Figure 3.1: Conical monopole with hemiellipsoidal dome.

In the figure, the geometry has been parameterized to better describe the antenna behavior and ease the optimization. The lowest resonant frequency, the most critical when the size is constraint, is given by the largest cone lateral length and the dome perimeter in this axis, and the associated wavelength is expressed in 3.1.

$$\lambda_{low} \propto 4\left[\frac{h_{cone}}{\cos(\alpha/2)} + \frac{l_{el}}{4}\right] \tag{3.1}$$

In the previous expression, α corresponds to the cone angle for the largest dimension and l_{el} is the the perimeter of an ellipse defined by R_U and R_N, which can be calculated by means of the Ramanujan approximation [41] as described in 3.2.

$$l_{el} \approx \pi\left[3(R_U + R_N) - \sqrt{(3R_U + R_N)(R_U + 3R_N)}\right] \tag{3.2}$$

The cone vertex is cut at a certain height from the ground plane, h_{feed}, which will determine the highest resonant frequency, with a proper diameter to connect the feeding SMA inner conductor. In practice, this section will be slightly larger due to the manufacturing process requirements.

$$\lambda_{high} \propto 10h_{feed} \tag{3.3}$$

The input impedance of a conical antenna fed by a coaxial line can be defined as [42]:

$$Z_{in} = Z_0 \frac{1 - \beta/\delta}{1 + \beta/\delta}\,, \tag{3.4}$$

where

$$Z_0 = 60 \ln \cot \frac{\alpha}{4}\,, \tag{3.5}$$

and β/δ corresponds to the ratio of reflected and outwardly propagating Transverse electromagnetic (TEM) waves in the region of the antenna.

3.2 Numerical Modeling and Design Optimization

The first step in the manufacturing process is to model the antenna with a simulation software and validate the chosen design. For this purpose, FEKO is chosen [43], since it provides powerful tools for high frequency simulations and for the optimization stage.

Figure 3.2 shows all the available solvers and their suitability depending on the model.

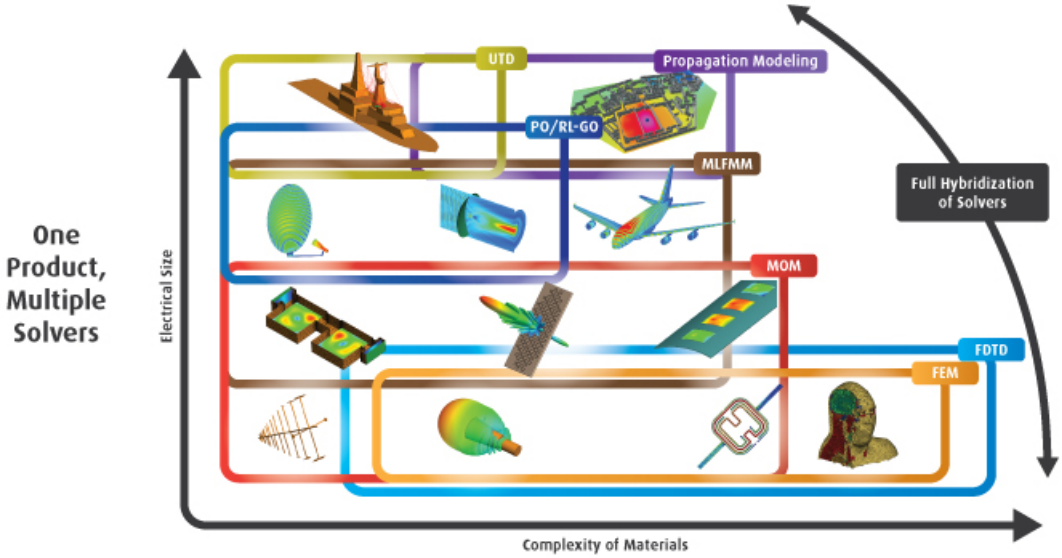

Figure 3.2: FEKO solvers diagram [44].

As first step, a model of ellipsoidal cone is created according to the requirements described in the previous section. By means of the optimization tool provided by the software, the cone height and the hemiellipsoid dimensions are optimized in an iterative process until a sufficiently good solution is found. Table 3.1 defines the optimization criteria.

Table 3.1: Optimization criteria.

Parameter	**Min value (mm)**	**Max value (mm)**	**Step size (mm)**
R_U	15	30	0.1
R_V	5	15	0.1
R_N	5	15	0.1
h_{cone}	15	30	0.1

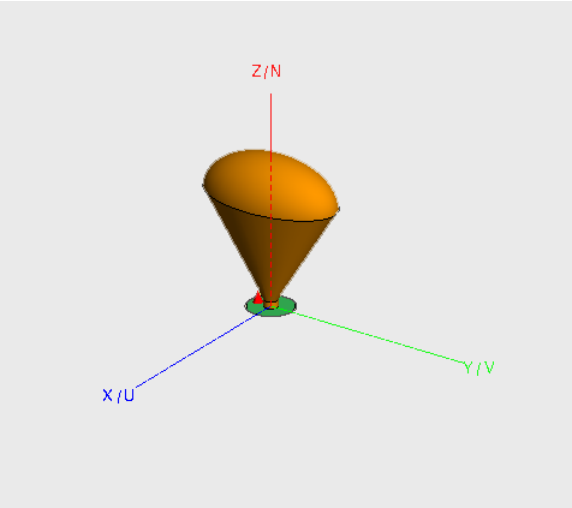

Figure 3.3: Environment used for the antenna simulation and optimization, including a ground plane and the SMA feeding.

All simulations, including those in the optimization stage, are performed with the following elements, also represented in Figure 3.3:

- The antenna, modeled with a Perfect Electric Conductor (PEC) cone and the dome of the same material,
- A PEC ground plane of 30 cm×30 cm. The antenna is centered in the middle, with a vertical separation corresponding to h_{feed}.
- A coaxial SMA connector. The outer and inner conductors are modeled with PEC, whereas the dielectric insulator is made of PTFE, i.e., Teflon ($\epsilon_r = 2.1$). The connector is inserted in a hole on the ground plane, at the same coordinates as the antenna, and the inner conductor is raised until the cone cut vertex. The connector dimensions are specified in Figure 3.4, which are extracted from the original connector datasheet.

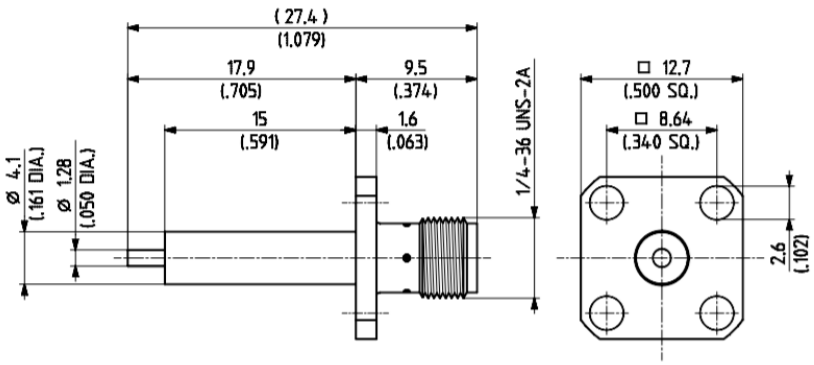

Figure 3.4: SMA connector dimensions [45].

After the optimization process to fulfill the previously mentioned requirements, the software provides the values depicted in Table 3.2.

Table 3.2: Antenna parameters after optimization.

Parameter	**Value (mm)**
R_U	29.9
R_V	17.1
R_N	8.9
h_{cone}	21.8
h_{feed}	1.5
D_{SMA}	1.28

Once the dimensions are obtained, the design is evaluated at different frequencies. The UWB performance is validated by means of the S11 parameter, which is simulated for a large frequency range (see Figure 3.5).

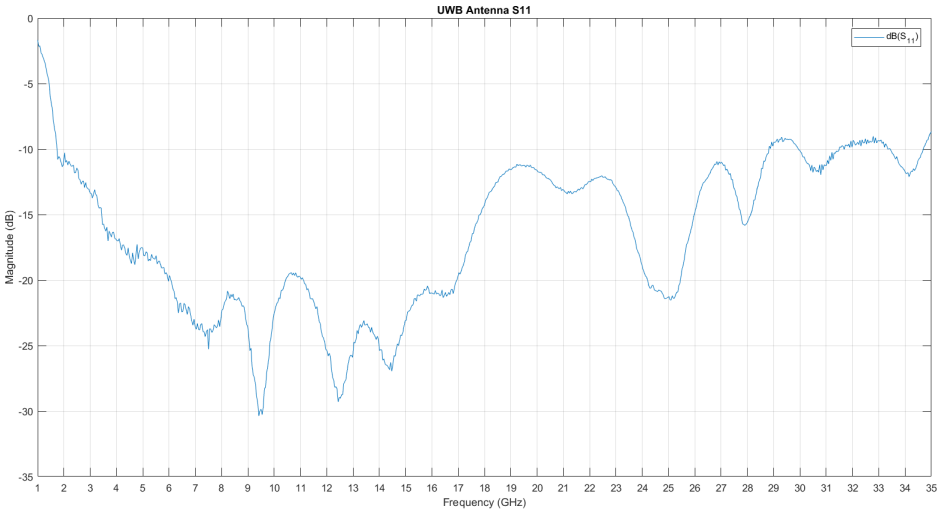

Figure 3.5: Antenna S11 parameter with SMA feeding between 1 and 35 GHz.

On the other hand, the radiation pattern is analyzed at the bands of interest. In particular, Figure 3.6 represents co- and cross-polar patterns for XZ and YZ plane at 3.6, 5.9 and 26 GHz, the central frequencies of the most promising bands for next-generation of mobile communications, as it was detailed in previous chapters. A null in the vertical axis and maximum radiation in the horizontal plane are expected, since it is a monopole in essence.

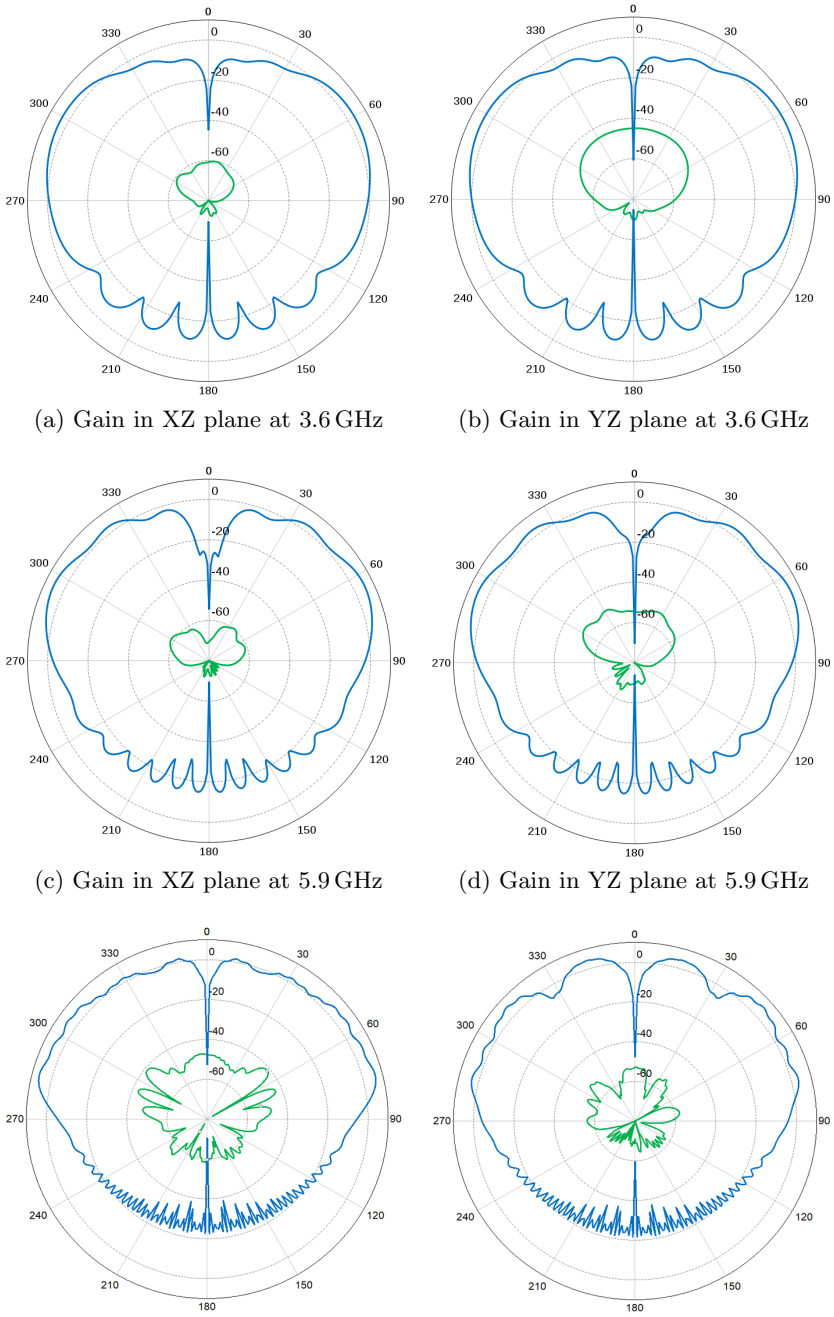

(a) Gain in XZ plane at 3.6 GHz

(b) Gain in YZ plane at 3.6 GHz

(c) Gain in XZ plane at 5.9 GHz

(d) Gain in YZ plane at 5.9 GHz

(e) Gain in XZ plane at 26 GHz

(f) Gain in YZ plane at 26 GHz

Figure 3.6: Co- (theta, blue) and cross-polar (phi, green) gain patterns.

The radiation is close to the expected, but it is possible to determine a small, wide peak between 60° and 70°. This is due to the antenna geometry, which has an angular aperture that produces a variation in the radiation pattern respect to the ideal monopole. In any case, for theta angles between 30° and 90°, gain is above 0 dBi. Regarding cross-polar gain, it is larger in the YZ plane, at both frequencies. In general, radiation is degraded as frequency increases.

Finally, the phase variation of the reflection coefficient over frequency is represented in order to verify its linearity.

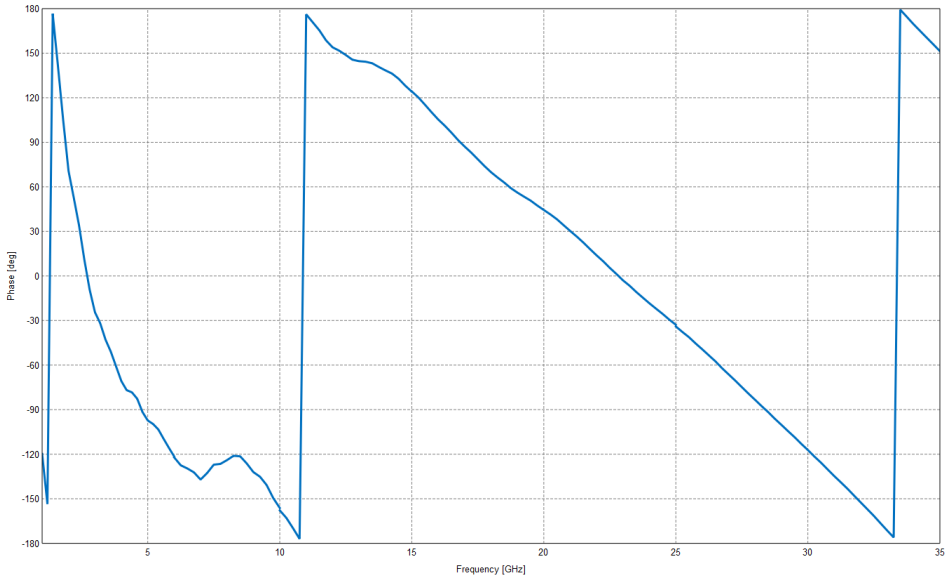

Figure 3.7: Phase of the reflection coefficient between 1 and 35 GHz.

Figure 3.7 shows a practically linear tendency for frequencies above 10 GHz, but the variation below that frequency is sharper, specially around 8 GHz. Nevertheless, the antenna is intended to be operative at different frequencies but with limited bandwidth values, thus in local terms it can be assumed to be linear at the desired frequencies.

3.3 3D-printing and manufacturing

The final manufacturing of the antenna is made by means of the 3D-printing technique. The basic idea is to create the geometry of the design in plastic and metallize the surface to make radiation possible. The most challenging part is to ensure the connection between the feeding and the metallizing. In consequence, the design is slightly modified to insert the connector inside the cone.

The end of the SMA inner conductor is soldered to a drilled screw and a thread of the appropriate diameter is inserted into the cone. During the process, the conducting layer is also applied to the thread and the electric continuity is ensured. Figure 3.8 shows the plastic geometry previous to the metallizing, with the inserted thread, and the modified SMA.

(a) 3D-printed geometry with inserted thread (b) SMA connector with soldered screw

Figure 3.8: Printed geometry and modified connector.

Once the basic geometry is created, the metallizing process starts. It consists of three main steps:

1 Application of conducting paint
A spray is used to cover the entire surface, as homogeneously as possible, with conducting paint. It contains copper particles that will allow current to flow along the antenna surface and radiate.

2 Copper deposition
The painted antenna is submerged in a tank with metallizing liquid. Its composition is described in Table 3.3. This step lasts 24 minutes, the required time to obtain a 17 µm layer, corresponding to a Printed Circuit Board (PCB) standard thickness. The liquid and the antenna are both connected to the electrodes of a power supply, which provides a current proportional to the surface ($3\,\mathrm{A/dm^2}$).

3 Application of tropicalizing varnish
Finally, to prevent the metallizing from rusting, a varnishing spray is applied. The varnish is a tropicalizing liquid that creates thin coating around the antenna and eases its handling.

Table 3.3: Metallizing liquid composition (for a 30 l tank).

Component	**Quantity**
Distilled water	14.3 l
Sulfuric acid	3.5 l
Sodium chloride	4 g
Bungard Elektronik's CU400C	12 l
Bungard Elektronik's CU400A	180 ml

(a) Antenna after applying the conducting paint.

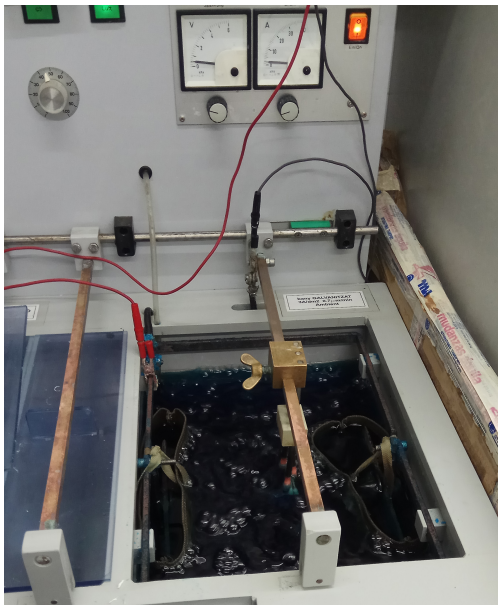

(b) Metallizing tank during operation.

(c) Tropicalizing spray.

Figure 3.9: Sample pictures of the metallizing process.

3.4 Antenna measurements

The metallized antenna must be analyzed now to validate its performance compared to simulated results. It must be stated that the initial model used a solid PEC antenna, whereas the real antenna is essentially a conducting surface on a plastic shape. Therefore, some discrepancy may be observed. The goal of the following measurements is to quantify this divergence and conclude whether the manufacturing process is valid or not.

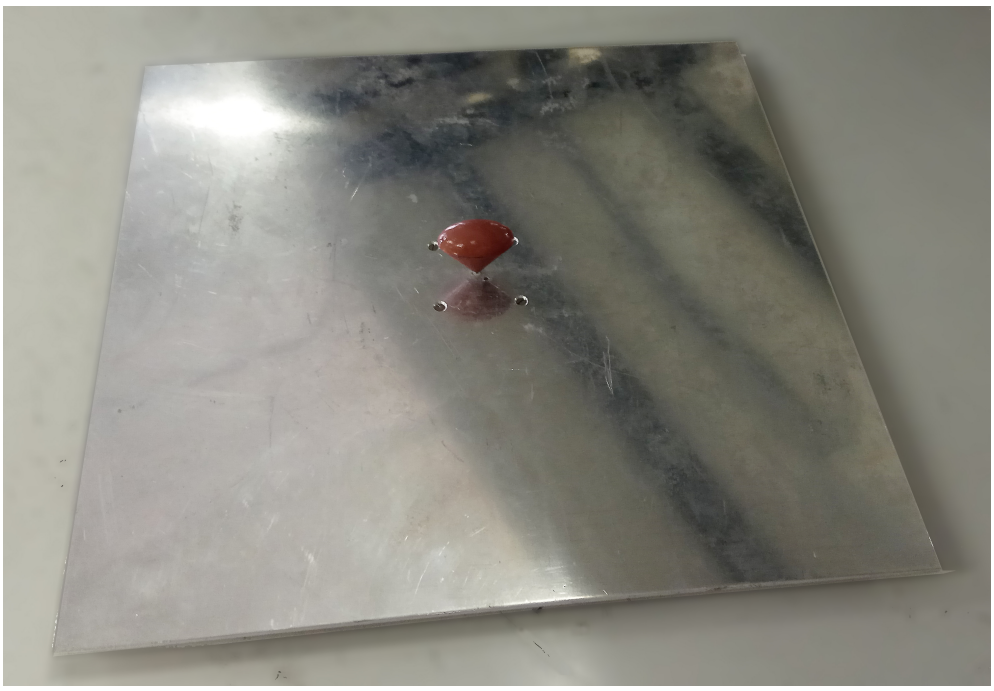

Figure 3.10: Testing set-up, including the antenna, the SMA connector and the 30×30 cm ground plane.

The first parameter to be measured is the S11. Input reflection coefficient defines the matching of the entire structure, shown in Figure 3.10, and it can be affected by several aspects: the antenna geometry, the feeding type, the connector or even the ground plane. The simulations already considered a finite ground plane (30×30 cm), but not the real material, since it was also modelled as a PEC surface. In any case, this is not expected to be the main reason of discrepancy.

Figure 3.11 shows the measured and the simulated values of the S11, both magnitude and phase. Due to limitations in the calibration procedure, only frequencies up to 26 GHz are considered. Regarding return losses (magnitude), the behavior is really close to the expected until 12 GHz, approximately. From then, the measured values are much more abrupt, specially around 14 GHz, where a peak is almost crossing the 10 dB threshold. On the other hand, phase is not as linear as expected and some sudden variation can be observed, for example, at 16 GHz. The different phase slopes indicate a difference on the origin (reference) point.

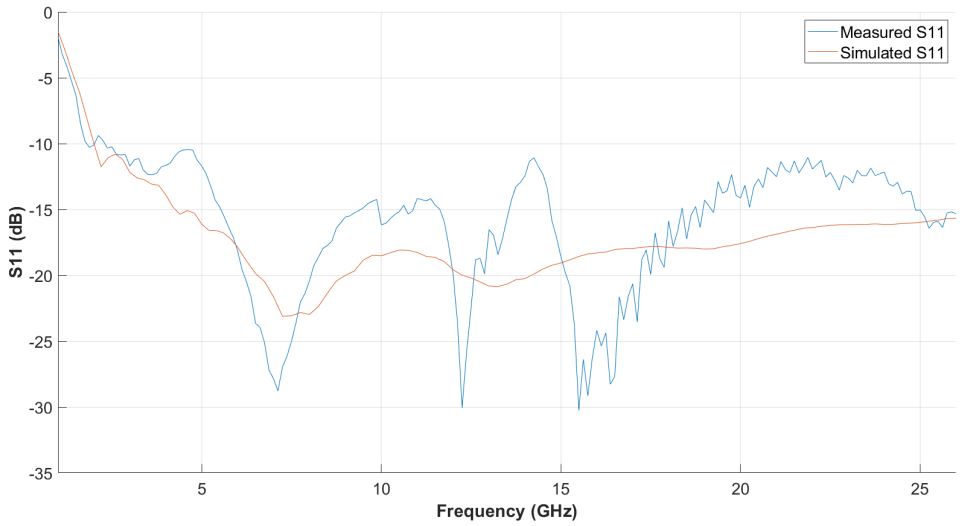

(a) S11 magnitude.

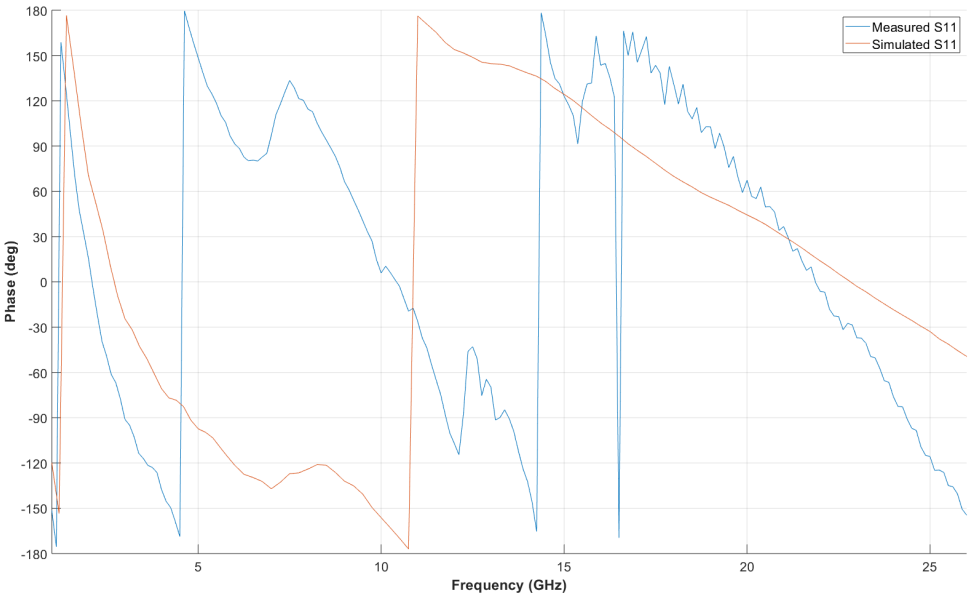

(b) S11 phase.

Figure 3.11: S11 measured vs. simulated values from 1 to 26 GHz

The S11 measurements were performed with a Vector Network Analyzer (VNA) inside the laboratory, which is not a reflection-free environment. This may be also another source of error, despite the surroundings of the antenna were kept as clean as possible from obstacles. A much more precise analysis could be done using an anechoic box to place the testing set-up.

Finally, the radiation pattern is measured at the anechoic chamber for the two sub-6 GHz frequencies. The measurement is not performed at the mmWave band due to limitations in the RF connections, but it is expected to be done in the following months.

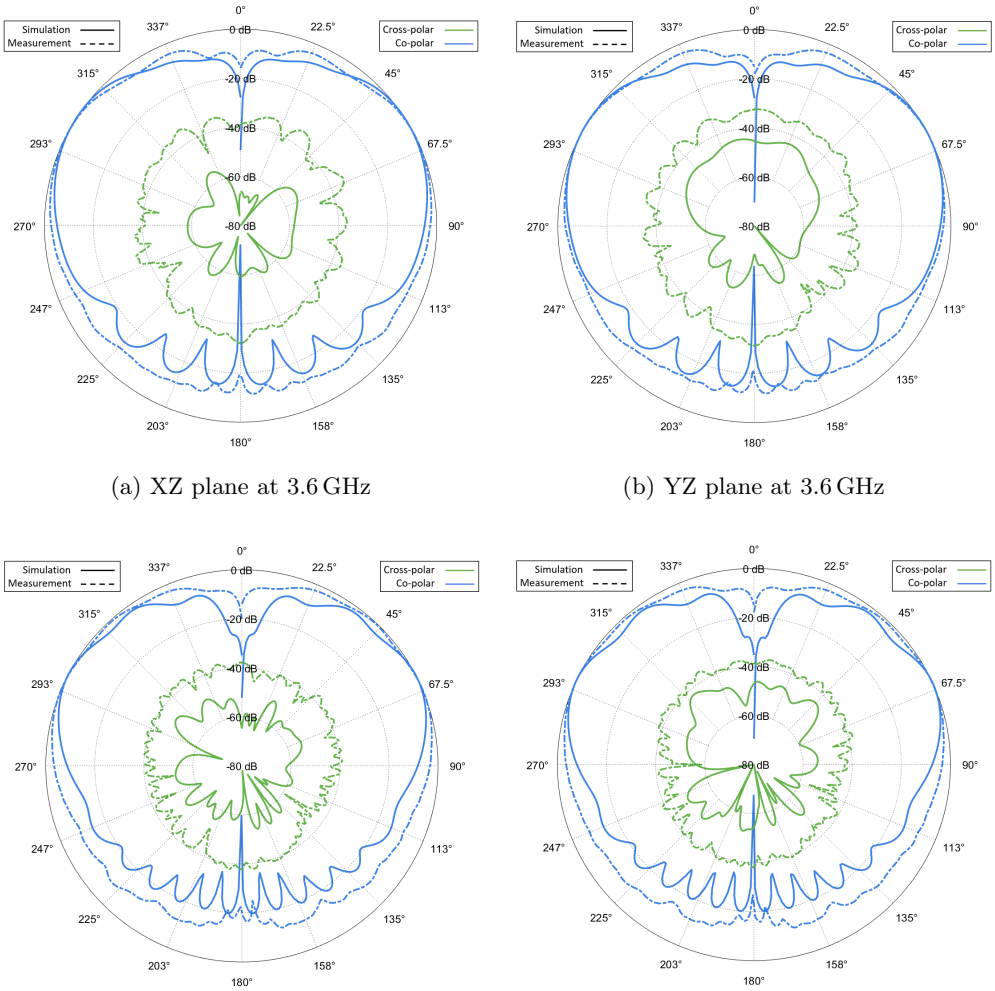

(a) XZ plane at 3.6 GHz

(b) YZ plane at 3.6 GHz

(c) XZ plane at 5.9 GHz

(d) YZ plane at 5.9 GHz

Figure 3.12: Co- (theta) and cross-polar (phi) normalized radiation patterns.

Figure 3.12 shows a good agreement between the measured and simulated patterns for the co-polar component. On the other hand, cross-polar radiation is between 10 and 20 dB higher than expected.

3.5 Multi-antenna Geometries

The final goal of this work is to design, validate and implement a MIMO system to provide an enhancement in terms of capacity for future 5G cellular communications. In consequence, several antennas must be considered at each end. This leads us to a multi-antenna geometry that has to be developed with the recently described monopoles.

MIMO systems are then compared with Single Input Single Output (SISO) for different cases:

- **MIMO 2x2**. The user, a vehicle for instance, mounts two monopoles, with a separation d between feeding points. They are aligned in the axis corresponding to the R_U dimension.
- **Linear MIMO 4x4**. Four monopoles are mounted on a line, separated a distance d between them. They are aligned in the axis corresponding to the R_U dimension.
- **Square MIMO 4x4**. Four monopoles are divided in two columns. The separation between columns is the same than the inter-element distance for each one. The two antennas in the same column are aligned along the R_U dimension, whereas each row corresponds to the R_V axis.

Figure 3.13 depicts the three multi-antenna geometry use cases.

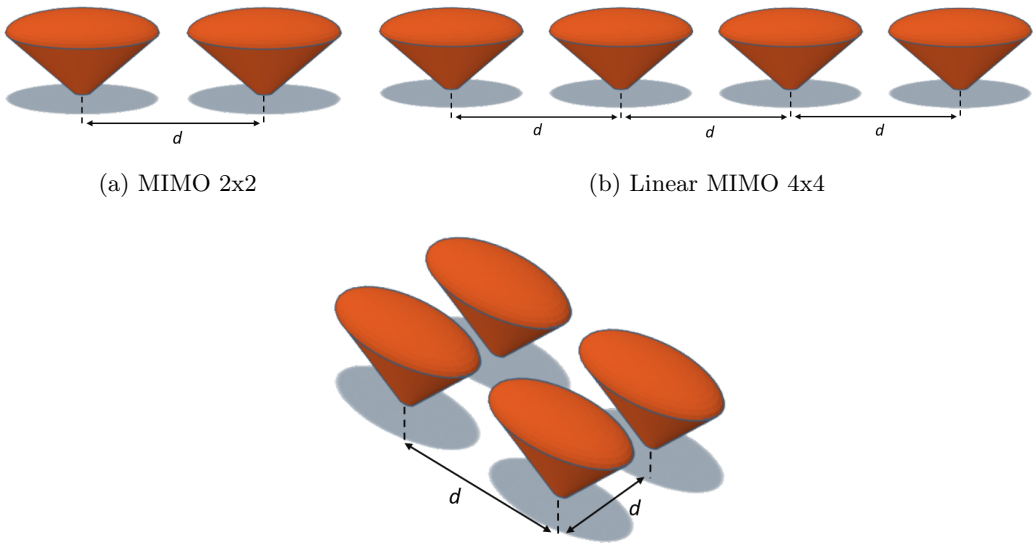

(a) MIMO 2x2

(b) Linear MIMO 4x4

(c) Square MIMO 4x4

Figure 3.13: Multi-antenna geometries.

In Chapter 5, the performance of each geometry is discussed in the context of a V2I communication for an urban environment.

Chapter 4

Indoor Mobile MIMO Channel Modeling

In this chapter, the channel characterization of an indoor scenario is discussed as one of the possible cases of a 5G communication. Indoors are much more controlled environments compared to outdoors and they exhibit very particular propagation properties. In this case, a portion of a corridor is chosen, with close and high walls, where rays are confined. A simulated approach is required before the experimental validation and an accurate model must be defined. Then, the model is confirmed by performing empirical measurements on the real scenario that was simulated before.

The essence of the study concerns the comparison of single and multi-element geometries. Commercial propagation-based simulation tools are used to create the model and validate the channel performance by means of its propagation matrix. According to the final results, validated with real measurements afterwards, a threshold on the MIMO order can be defined based on the capacity improvement. The increased complexity of such a system must be justified by a true gain, otherwise the use of conventional single element geometries must be kept.

Regarding next-generation networks, three frequency bands according to the technology lying on it are of the interest of study: the LTE-based cellular systems at 3.6 GHz, the 802.11p band at 5.9 GHz under discussion for DSRC and WiFi spectrum sharing [46] and the 26 GHz band devoted for future 5G networks. Using identical systems, the performance of the MIMO channel is analyzed for the three cases.

4.1 Simulated Model of an Indoor MIMO 5G System

The first step to evaluate a communication system consists in designing a virtual model of the final testing environment and perform the same calculations for a simulated scenario. In this way, several parameters can be tuned and an certain performance can be expected from the experimental measurements. In consequence, rigorous models must be used to obtain reliable and meaningful results.

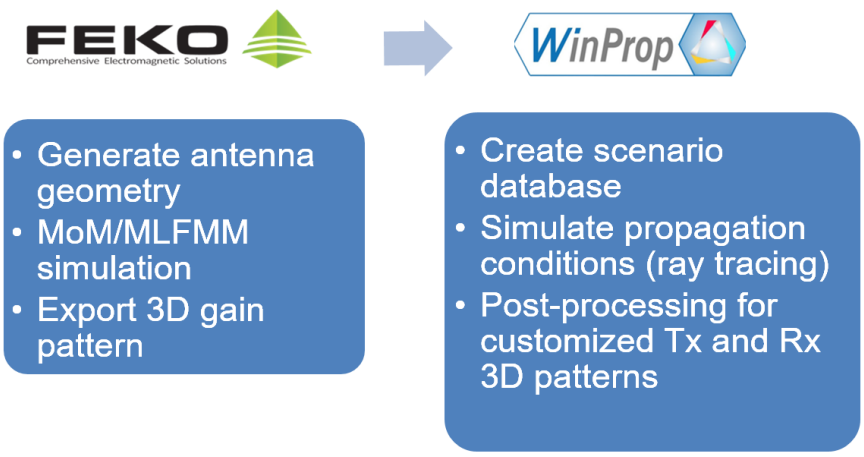

Figure 4.1: Two-step simulation procedure.

The simulation can be defined as a two-step procedure. First, antennas are evaluated at the desired frequencies by means of a computational electromagnetic software, FEKO, as previously done in Chapter 3. The same UWB cone-like monopole is used, with minor modifications to match the real shape of the manufactured antenna, which required an enlarged base to screw the connector. The antenna is simulated on a 30 cm×30 cm ground plane and fed with a coaxial SMA connector. The software includes a fast solver for high-frequency, large-size simulations based on Method of Moments (MoM) called Multilevel Fast Multipole Method (MLFMM). It is more accurate than Physical Optics (PO) or asymptotic techniques.

In second term, the generated pattern is used in WinProp, the wave propagation tool, to perform channel simulations for the indoor environment. A scenario is created to model similar to the real one, regarding both shape and material properties. Propagation is simulated using the ray tracing technique, later explained in Section 4.1.2, for omnidirectional transmitting and receiving antennas. Then, customized patterns are used to weight the rays at a post-processing stage, which reduces drastically the number of channel simulations required, and hence the computation time, making possible to reuse the same interactions for different antenna geometries.

4.1.1 Design of the Indoor Scenario

The scenario used in the study is the basement of the D3 building, at the university campus. The most important feature is the narrow corridor, of 1.62 m width. In addition, small hall is located at the end, where the staircase to the ground floor begins. It is used to define the NLOS section, since the transmitter is located at the middle of the corridor. Line of Sight (LOS) communication can be established along the entire corridor until the hall.

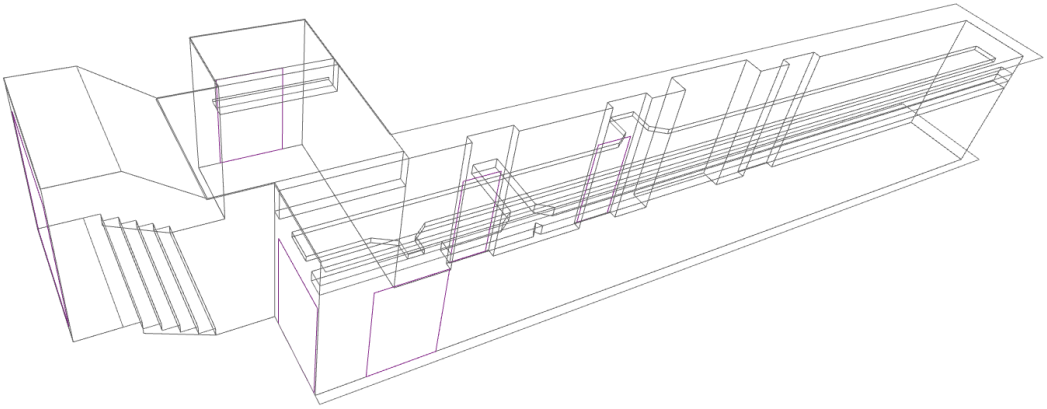

Figure 4.2: Scenario of the D3 basement.

Walls are defined with 3.1 m height and made of brick, of 20 cm thickness. Five doors can be found at different positions. Two of them are metallic, two are wooden, 2.06 m height for both cases, and one is made of glass, corresponding to the main exit after the stairs and it is 2.5 m height. The stairs imply an extra elevation of the ground of 0.87 m respect to the reference level.

Some metallic beams are located below the rooftop, used to pass cables along the corridor and place the WiFi routers, and they are also included in the model, since their impact may be noticeable on the propagation of waves. The elevator is located next to the transmitter position, which is defined fixed at the coordinates origin. It is also modeled with metal and the entire structure arrives to the ceiling, with a total width of 2.06 m. Figure 4.2 shows the sketch of the scenario modeled using the simulation software.

4.1.2 Ray tracing approach

The ray tracing procedure [47,48] basically consists in defining rays (paths) from the source to the observed positions, assuming different interactions with the objects in the environment. It takes into account up to four types of rays:

- **Direct rays**. Directly from the source to the receiving point, corresponding to LOS propagation paths.
- **Reflected and transmitted rays**. At the interface between two mediums, two rays are generated: one reflected in the first medium and another transmitted to the second. Specular reflection using Geometrical Optics (GO) approximation contributes to the computation of the field.
- **Diffracted rays**. A single incident ray generated a large amount of possible diffracted rays when reaching an edge. They are arranged forming the so called Keller cone and can be defined by means of the Geometrical Theory of Diffraction (GTD).

- **Scattered rays**. They appear when a ray arrives at a rough surface and their contribution can be much lower compared to previous cases, as the behavior may be totally random.

All these interactions can be combined in multiple surface-surface reflections and surface-edge or edge-surface relfection-diffractions. Every interaction added to the model increases the complexity, and therefore the computation time, but it provides a higher degree of accuracy. Thus, a trade-off between calculation and rigorousness must be considered.

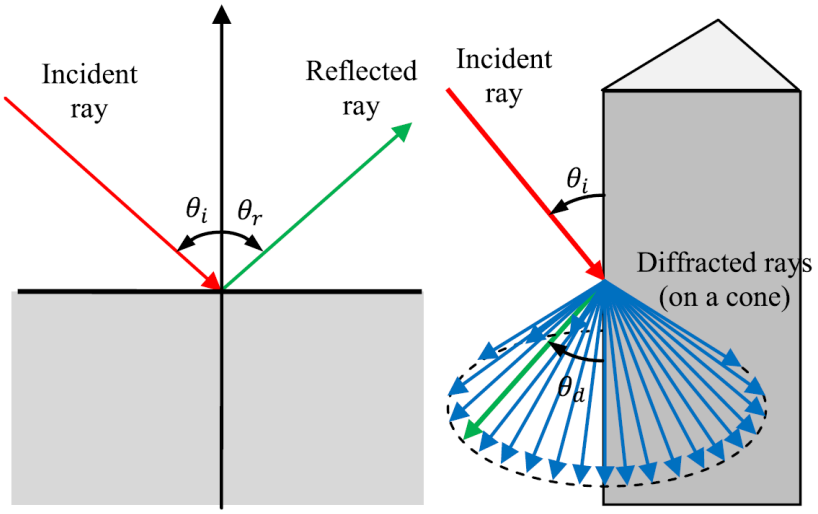

Figure 4.3: Ray tracing interactions: reflected ray on a planar interface (left) and diffracted cone of rays at an edge (right) [48].

The channel transfer function between the i-th transmitter and the j-th receiver of a MIMO system is obtained as the addition of all multipath contributions between them and can be expressed as follows:

$$h_{ij}(\boldsymbol{r}) = \sum_{t=1}^{T} \Gamma(\boldsymbol{r_t}) e^{-j\boldsymbol{k}\cdot\boldsymbol{r_t}} \,, \tag{4.1}$$

where $\Gamma(\boldsymbol{r_t})$ is the complex envelope of the channel transfer function for the $\boldsymbol{r_t}$ multipath distance vector and $k = 2\pi/\lambda$ is the wave number.

4.1.3 Antenna Set-up

The goal of this study is the analysis of multi-antenna geometries for 5G frequency bands at a physical level. The channel is characterized for three different cases according to the number of antennas. SISO, MIMO 2x2 and MIMO 4x4 are tested using the design proposed in Chapter 3.

The system is completely symmetric, since both transmitter and receiver have always the same number of elements, using the same antennas with the same layout. The

antennas are mounted on a metallic plane at 1.5 m from the floor. For multi-element cases, the radiators are placed on a line with a fixed inter-element distance for all frequencies of 8 cm. This corresponds to half the wavelength at the lowest frequency (3.6 GHz) between the cone edges for the largest dimension. In terms of wavelength, the antennas are further from the others as the frequency increases. In consequence, smaller correlation is expected for higher bands [49, 50]. Figure 4.4 shows the multi-element geometry previously described.

The only variation is the receiver position, that is moving according to a certain trajectory following the corridor up to the hall stairs. Then, two main regions can be defined: LOS along the corridor and NLOS once the receiver has turned the corner.

Transmission power is set to 0 dBm always. In case of several radiators, it is equally divided for all them. The noise level is estimated to be -90 dBm for the simulated environment.

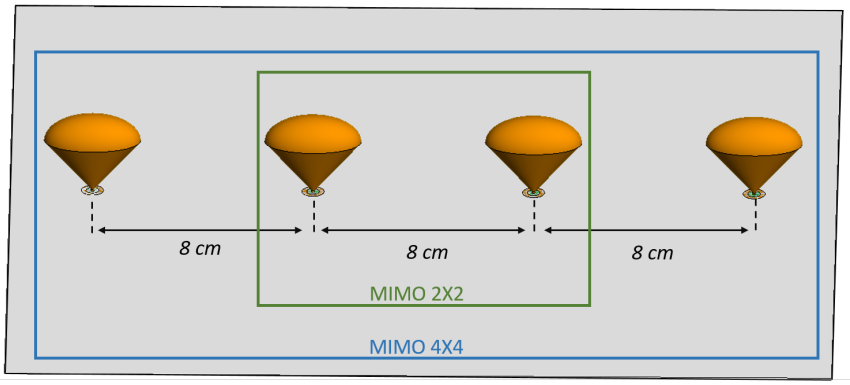

Figure 4.4: Multi-antenna set-up for MIMO 2x2 and MIMO 4x4.

4.1.4 Simulation Results

The first parameter to analyze is the received power. It mainly depends on three factors: transmitted power, path loss and multipath. Power at the transmitter is kept constant, thus the comparison is always fair independently from the geometry. Free-space path loss is basically determined by the distance travelled by the wave and the wavelength, assuming that propagation is carried out in a homogeneous medium. This is not always true, but propagation through walls is negligible, since the attenuation of transmitted rays is extremely high, specially at mmWave band. Antennas are always the same and their directivity is almost constant for all the studied range of frequencies. The expression in (4.2) describes the well known Friis transmission equation [25].

$$P_R = P_T G_T G_R \left(\frac{\lambda}{4\pi R}\right)^2 \tag{4.2}$$

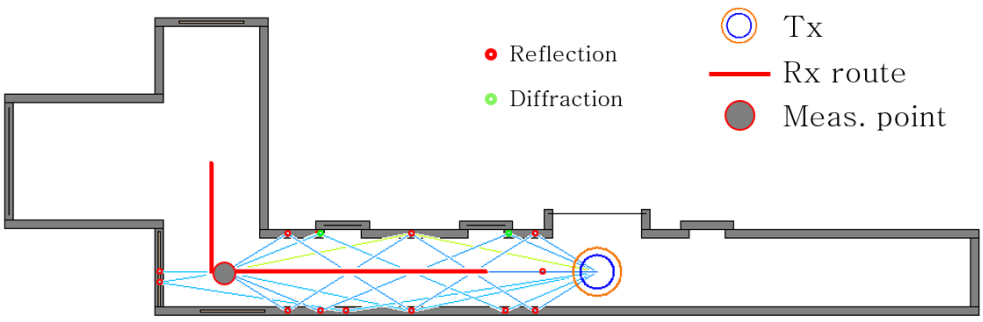

Figure 4.5: Example of multipath contributions at a given receiver position.

The multipath contribution is critical in indoor environments. The use of ray tracing software provides a tool to understand the contribution of each incoming wave to the final received power. Figure 4.5 shows different paths for a position of the receiver at the corner. In the case of a corridor, the walls act as a waveguide and rays are confined. The objects surrounding the antennas and the shape of doors and other elements can change the behavior of rays and constructive or destructive interference may be found when receiver is moved. This variations are more noticeable for high frequencies, when scattering randomness is higher.

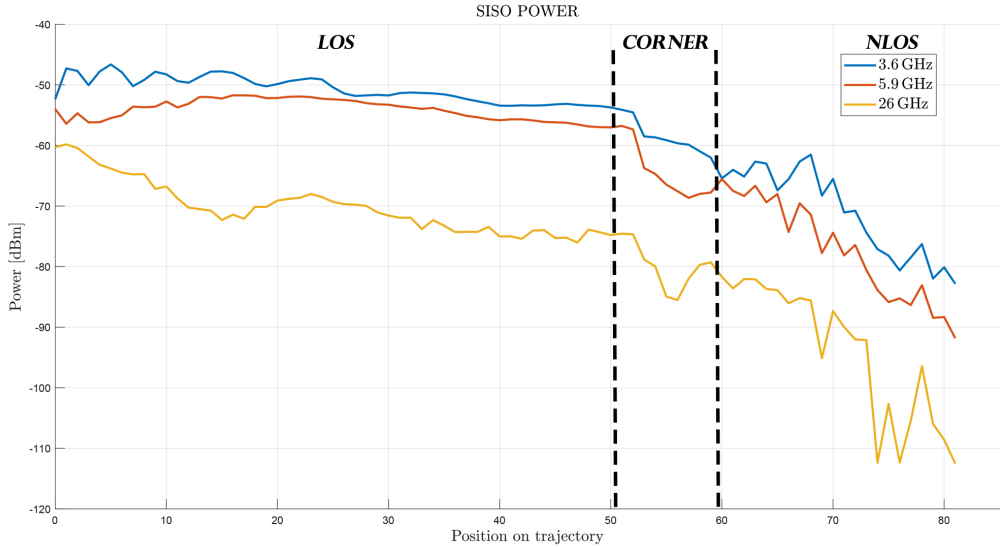

Figure 4.6: SISO received power as function of receiver position.

Figure 4.6 depicts the received power according to the receiver position for the three frequencies of study. Each position corresponds to a 10 cm displacement on the trajectory. The corner is located between position 50 and 60. In consequence, previous samples can be classified as the LOS region and the next ones, as NLOS. It can be stated that there is a great loss in terms of power for the case of 26 GHz. Received power is 10–20 dB lower compared to sub-6 GHz bands. This performance is in completely agreement with previous assumptions.

If the focus is put on the NLOS region, power decreases with a similar slope for the three cases but variations are sharper for the higher frequency. This also agrees with initial hypotheses.

Since the scope of the analysis are multi-antenna geometries, worthiness of using MIMO systems must be considered. Ideally, a pair of transmitting-receiving antennas should be established, independently of the rest, to obtain a number of uncorrelated channels equal to the MIMO order. In this way, the maximum capacity is achieved when the channel matrix, described in 4.3, is diagonal.

$$\begin{bmatrix} y_1 \\ \vdots \\ y_M \end{bmatrix} = \begin{bmatrix} h_{11} & \cdots & h_{1N} \\ \vdots & \cdots & \vdots \\ h_{M1} & \cdots & h_{MN} \end{bmatrix} \begin{bmatrix} x_1 \\ \vdots \\ x_N \end{bmatrix} \tag{4.3}$$

Equal diagonal elements imply equal constant eigenvalues. From a more practical point of view, the achievable capacity is given when eigenvalues are equally distributed and it defines a maximum threshold. Figure 4.7 shows the condition number, i.e., the ratio between the maximum and the minimum eigenvalues, for the three frequencies at each receiver position. To simplify the problem, only the MIMO 2x2 case is considered in this first stage.

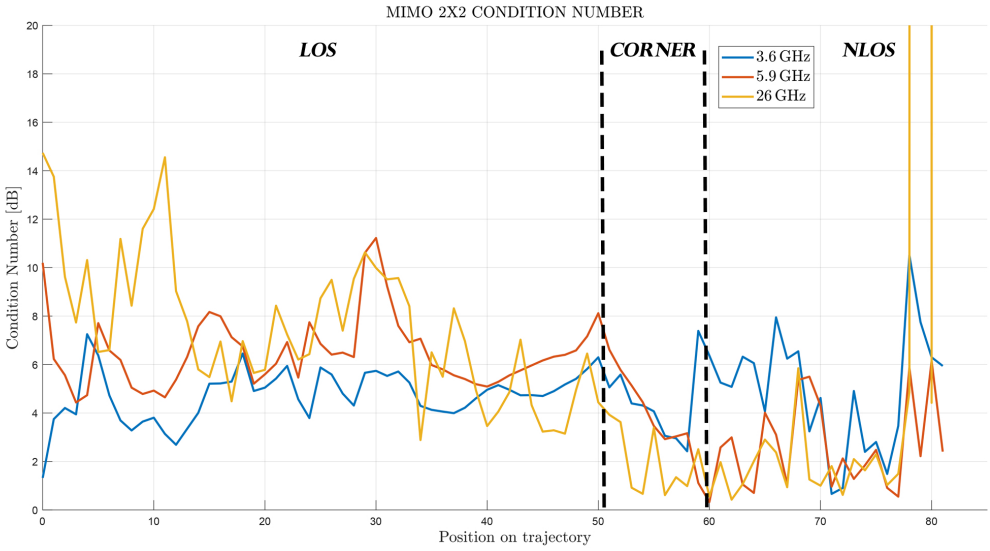

Figure 4.7: Condition number for MIMO 2x2.

Two different tendencies can be defined depending on the region. For LOS, condition number is higher for higher frequencies. It means that a more direct channel can be found and the use of several antennas may not be justified. On the other hand, when there is no direct view between transmitter and receiver, the behavior is inverted. Except for two particular positions, in which one eigenvalue is much smaller due to the specific reflections, in general, the condition number is around 2 dB both at 5.9 and 26 GHz, whereas the values for 3.6 GHz remain oscillating around 5 dB. This performance really demonstrates the scattering richness of NLOS environments, specially at high frequencies. The disadvantage is the low received power, that could make communication unfeasible.

The combination of power and MIMO channel determines the capacity. It can be described in terms of the channel matrix or directly with its eigenvalues, as shown in (4.4) and (4.5) extracted from [51].

$$C = log_2\left(det\left[\boldsymbol{I}_N + \frac{P_T \boldsymbol{H}\boldsymbol{H}^*}{P_N}\right]\right) \tag{4.4}$$

$$C = \sum_{i=1}^{N} log_2\left(1 + \frac{P_R \lambda_i}{P_N}\right) \tag{4.5}$$

In this case, λ_i corresponds to the eigenvalues of the product between **H** and its transpose conjugate, **H***, normalized to the Frobenius norm. P_T and P_N are transmitted and receiver noise power, respectively.

To evaluate the real improvement of using several antennas, the capacity can not be directly compared for the three frequencies. The absolute values can diverge noticeably, since propagation losses are completely different. Then, the figure of merit that can be common to all cases is the MIMO gain, i.e., the increment in capacity respect the SISO case. It is defined in (4.6).

$$\Delta C = \frac{C_{MIMO}}{C_{SISO}} \tag{4.6}$$

Figure 4.8a shows the MIMO gain for the 2x2 case. As expected from the condition number analysis, in LOS conditions the improvement is higher for lower frequencies. Only a peak around the sample number 35 is found for 26 GHz, but it may be produced by a destructive interference for the SISO geometry, which decreases the capacity that is in the denominator of previous expression. Around the corner, there is a curious effect for all frequencies. The gain is reaching a maximum in the three lines with a value of ΔC=1.8. The corner diffraction and the 90 degrees shape of the corridor are generating a region of strong reflections that improve the capacity. After the corner (NLOS region), MIMO gain is higher for the highest frequency and the other two follow a very similar trace.

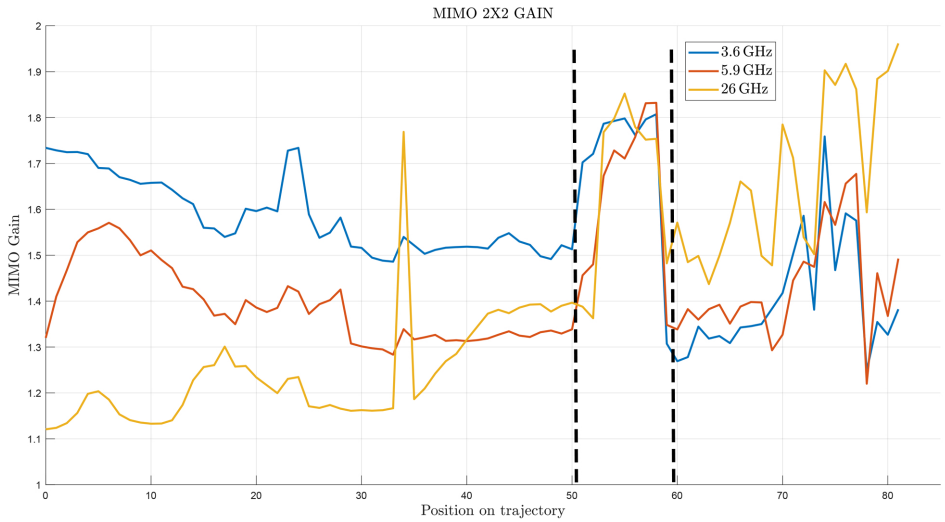

(a) MIMO 2x2.

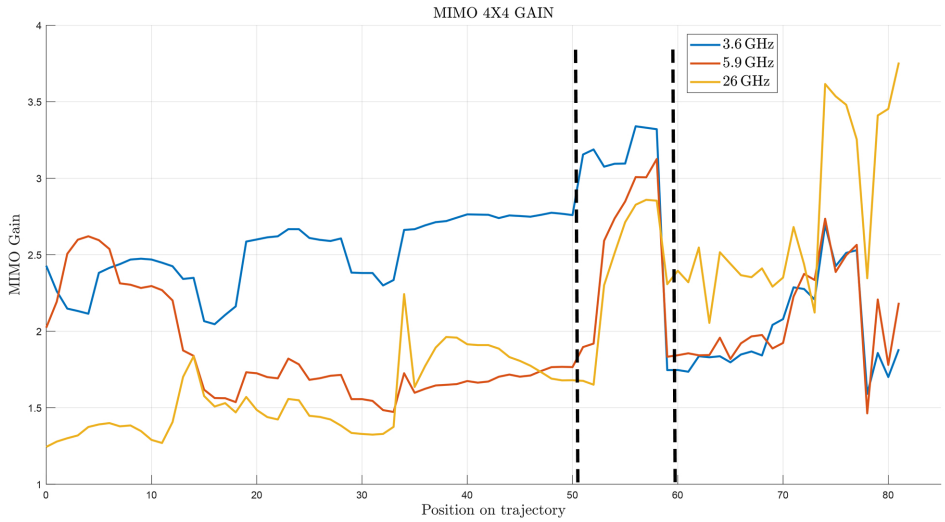

(b) MIMO 4x4.

Figure 4.8: MIMO capacity gain.

Figure 4.8b represents the same MIMO gain parameter but in the case of 4x4. The values in the graph are higher since the number of antennas is doubled but this ratio is not kept for the gain. In the LOS region, the three lines are almost confined between 1.5 and 2.5. At the corner, there is a peak again and, in the NLOS region, the gain is also higher for 26 GHz.

In consequence, at least for indoor communications, the use of a number of antennas greater than one seems to be limited according to the frequency. Lower bands present smaller losses and splitting our channel can improve the system performance. On the other hand, when frequency is increased, very rich scattering environments are required, but they are usually found in NLOS conditions, where losses are too high for a reliable communication. In this case, array structures can be proposed as a solution to overcome the path loss and group the antennas as a single radiator instead of dividing the channel.

4.2 Experimental Validation of the Indoor MIMO 5G System

The previous results have to be later validated by experimental measurements. The following lines relate the procedure to replicate the proposed model in a real environment.

4.2.1 Equipment set-up

The measurements are carried out at the basement of the D3 building at the *Campus Nord*. The channel sounding equipment has to cover a relatively small distance but the use of a wired solution for the transmitter-receiver synchronization is only possible for low frequencies due to attenuation and noise issues.

The central device for the measurements is a N5247A PNA-X VNA from Keysight Technologies. The device covers a frequency range up to 67 GHz and it can be used both at microwaves and the low part of mmWave bands. By means of the S-parameter calculations, the channel matrix can be extracted. Since this is a two-port device, only one transmitter and one receiver can be analyzed at a time. Two SP4T switches are used to connect up to four antennas (MIMO 4x4) at each side and the S21 parameter of each pair is measured. In particular, the Analog Devices ADRF5045 is used. The complete switch assembly is shown in Figure 4.9.

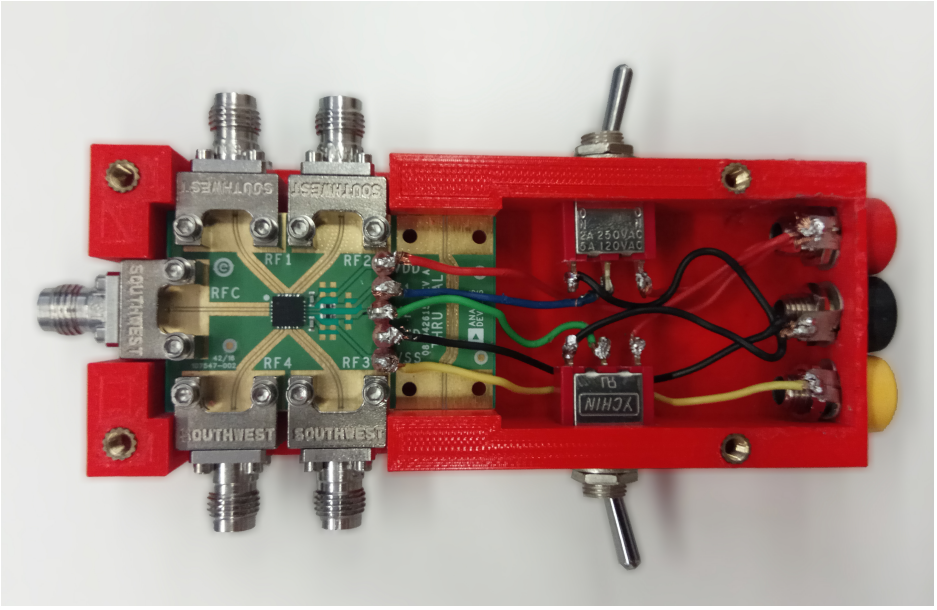

Figure 4.9: ADRF5045 SP4T switch.

Figure 4.10 shows the S-parameters of the switch measured with the VNA between 1 and 30 GHz when port 1 is connected to the common RF input and port 2, to one of the outputs, when the specific port is selected (a) or not (b).

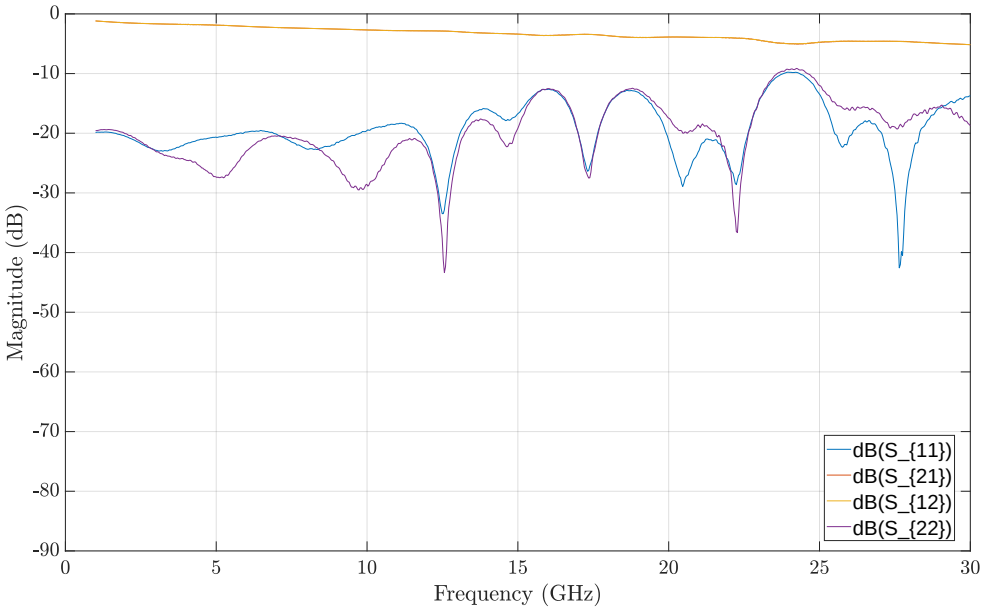

(a) Output selected.

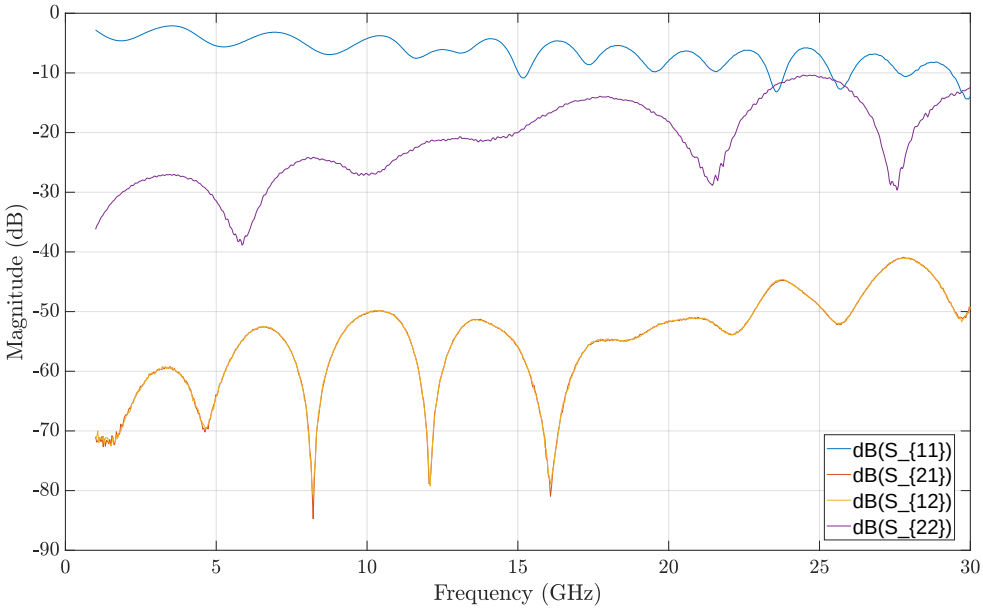

(b) Output not selected.

Figure 4.10: ADRF5045 S-parameters.

The transmitter is fixed at the center of the corridor and the receiver is moved following the same trajectory used in the simulations. The total distance to cover is 10.5 m and the VNA is fixed at the same position as the transmitter. Therefore, a solution must be found to properly connect the receiver to the analyzer port.

The first is a wired solution. It is only valid for the lowest bands considered in the study. The typical attenuation for commercial flexible coaxial cables is typically between 5 and 6 dB/m at 26 GHz. Those values make the wired connection unfeasible and

a second solution is proposed. In this case, two independent horn antennas optimized to work at the band of interest are used. They are isolated from the system under test and they are only used to connect the VNA port to the receiver switch.

Additional cables and adapters must be included since the antennas, switches and VNA ports connections are mismatched. Their impact has to be calibrated prior to performing the measurements. The complete set-up is depicted in Figure 4.11.

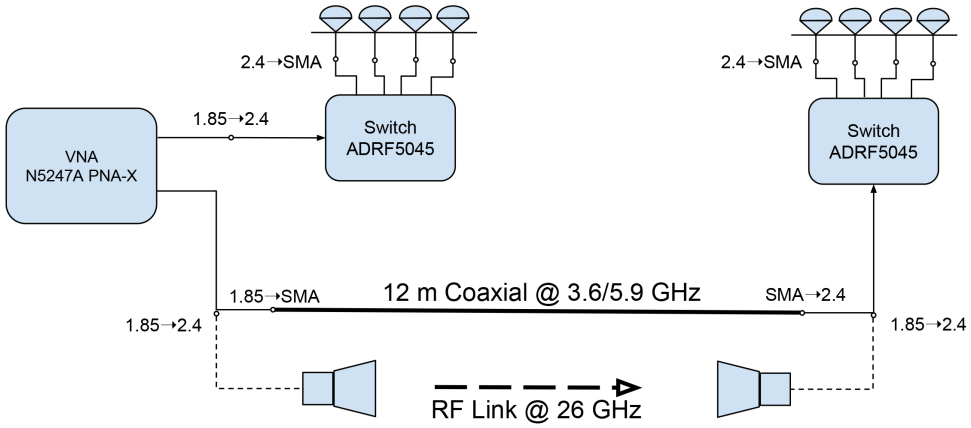

Figure 4.11: Indoor channel sounding set-up.

4.2.2 Measurement campaign

According to the initial project plan, the measurement campaign is scheduled to be performed on July 12$^{\text{th}}$. Due to a delay of the supplier in the delivery of the required cables, all tests are interrupted until the required material was fully available. A tight schedule can lead to this type of issues if unexpected delays are not properly considered in the project plan.

As a preliminary study, the sub-6 GHz SISO case is studied to get used to the methodology and obtain initial results. The S21 parameter is plot for the same trajectory, in this case sampled every 20 cm (41 samples), and the measured values are shown in Figure 4.12. Due to the large attenuation of the coaxial cable, which should be substituted by an improved model (or the horn set-up for mmWave frequencies), results after the corner, in NLOS condition, are not reliable due to the weak signal compared to noise. For the same reason, transmission power has been increased to 15 dBm.

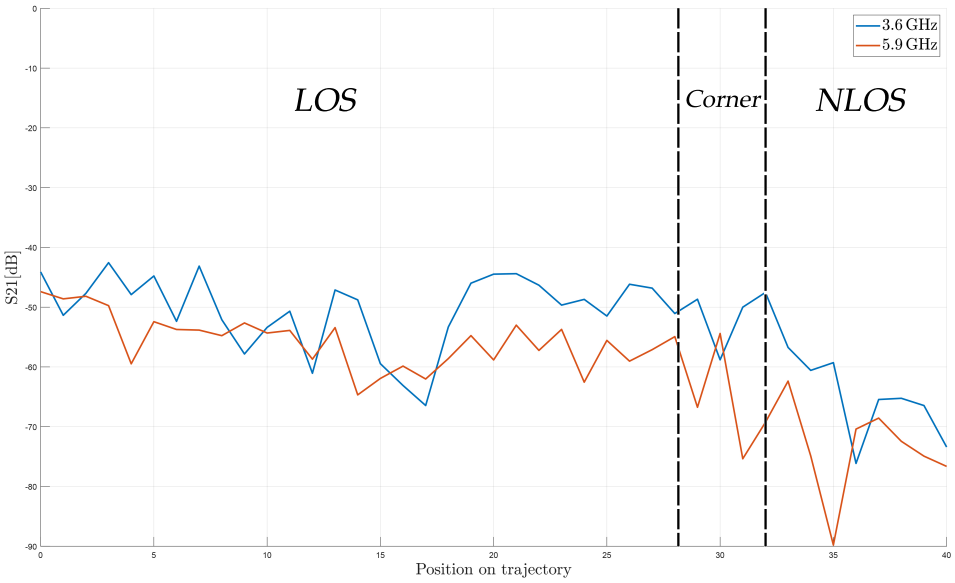

Figure 4.12: SISO sub-6 GHz S21 parameter.

By the date of defence of the thesis, the results are expected to be extended in order to validate the simulations and the consequent statements.

Chapter 5

V2X Channel Modeling of a Realistic Urban Environment

Multi-antenna geometries are able to improve the performance of mobile communication systems in terms of capacity. Especially, vehicular communications are an emerging field in the context of 5G and the implementation of MIMO configurations for automotive applications requires to consider a realistic propagation environment. In this chapter, the electromagnetic channel model for an urban scenario is investigated based on the achievable capacity, proposing different antenna geometries and analyzing them mounted on the vehicle. As radiating element, the UWB 3D monopole previously presented in this thesis is used, properly designed to operate from below 2 GHz up to K band. In particular, 3.6, 5.9, and 26 GHz bands will be compared regarding their performance for an urban V2I environment. These frequencies correspond to the European allocation of 802.11p, LTE and 5G future systems. Two of them are found below 6 GHz, were the spectrum is becoming more and more overcrowded, wheres the latter is close to the known as mmWave region, where larger bandwidth is available. All the details about standards and regulations can be found in Chapter 2.

Within the framework of connected cars, there is a growing interest in investigating novel wireless technologies to achieve faster data rates, ultra-low latency, and more energy efficient systems. As part of the new paradigm of mobile communications, they are a scope of research of the next generation of cellular systems. All these challenges involve the use of new frequency bands, and larger bandwidths. The consequence at physical level is the need of new electromagnetic models of the channel propagation and improved designs of the antennas.

Otherwise, in terms of channel capacity, a multi-antenna configuration can improve the system performance [52] and new geometries must be considered from the initial design. In order to study the effect of these new configurations, the analysis of the environment for a realistic urban vehicle communication is performed. The antennas are mounted on the rooftop of a car and it is moved along a certain trajectory. SISO capacity is then compared to MIMO 2x2 and 4x4 cases. For the last case, two geometries are proposed: a straight line along the longitudinal axis and a square shape. A dedicated section about MIMO antennas is found in Chapter 3.

5.1 Methodology

In order to compare the performance of the system using the distinct geometries, channel capacity is used as the figure of merit to evaluate the simulation results.

The capacity of a MIMO system may be obtained as [51]:

$$C = log_2\left(det\left[\boldsymbol{I}_N + \frac{P_T \boldsymbol{H}\boldsymbol{H}^*}{P_N}\right]\right), \tag{5.1}$$

where P_T and P_N are the transmit and noise power, respectively, I_N is the identity matrix for N receiving units, and $(.)^*$ denotes the transpose conjugate. The channel matrix $\boldsymbol{H}$ corresponds to the multipath relations between all input and output ports.

This channel matrix is obtained using a ray tracing approach by means of a software tool, WinProp, already presented in previous chapters, for the chosen urban scenario. The large environment to analyze, even for the lowest frequency considered in the study, makes unfeasible the use of any numerically exact solver and high frequency methods perform well enough.

Including the car geometry in the scenario also increases the complexity of the environment and reduces the accuracy of the real antenna radiation. In consequence, the antenna is simulated in FEKO (as seen in Chapter 3) mounted on the car using a combination between MoM and PO. Then, the radiation pattern is exported to WinProp to perform the propagation simulations.

The car also follows a certain trajectory. Its position is sampled and the capacity is calculated for each individual location, as explained in Chapter 4. Finally, the average, expressed in (5.2) for N_S samples, is considered in the analysis of the results as the figure of merit to evaluate the system performance.

$$C_{av.} = \frac{1}{N_S}\sum_{i=1}^{N_S} C_i \tag{5.2}$$

5.2 Urban Scenario

A realistic approach for the analysis of a car in an urban area is required to model the system and, in this case, a portion of a real city is chosen to simulate the V2I environment in WinProp. Fig. 5.1 depicts two crossing streets in the city of Barcelona, corresponding to the district of *L'Eixample* (characterized by its rectangular shapes and almost 90 degrees corners). The model is composed of an asphalt ground, five buildings, trees and traffic lights. Object materials are taken into account by the simulation tool in the computation. Therefore, buildings are 18 m height and made of concrete, trees are simulated with a wooden trunk and vegetation on top, which let the rays to pass through at the cost of additional attenuation, and traffic lights are metallic.

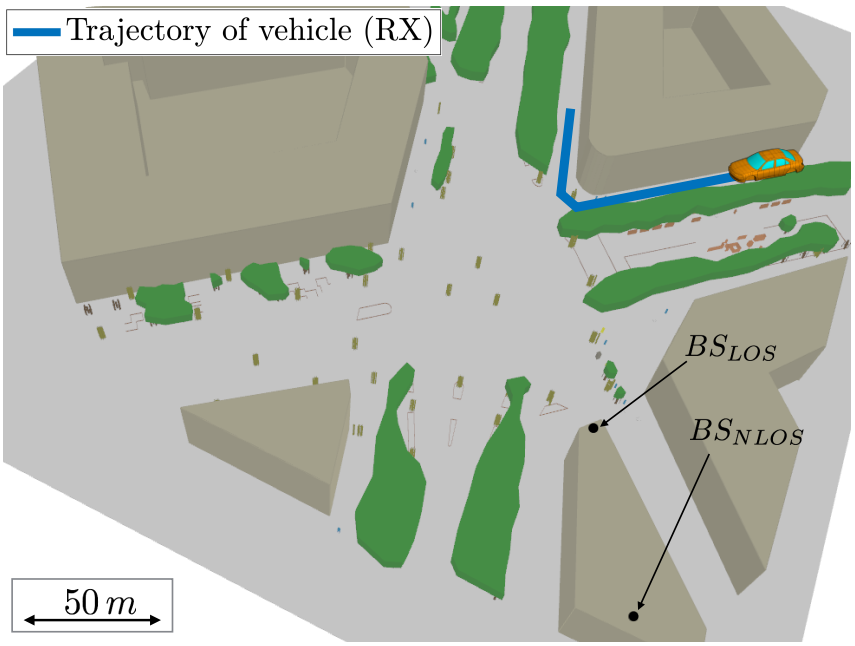

Figure 5.1: Simulated scenario of an intersection in Barcelona.

Two transmitting Base Station (BS) are defined to model two different types of communication: one with direct view to the car, or LOS, and another one for which the direct path is blocked by a building, i.e., NLOS. BS_{LOS} and BS_{NLOS} are placed on the top of the same building at the height of 21 and 20 m from the ground, respectively, with the difference that BS_{LOS} is closer to the car, whereas BS_{NLOS} is move backwards to block the car view. All BS consist of a set of ideal omnidirectional elements. One, two, or four antennas are used for SISO and MIMO 2x2 or 4x4 (linear and square) with a constant spacing of $\lambda/2$ at the corresponding operating frequency.

The receiver, the car, drives along a trajectory with a total length of 143.4 m, sampled every 0.1 m. Each sample represents a still position of the car, thus no Doppler effect is assumed in the analysis. The trajectory starts behind some trees, driving towards the main street where the BS is located, and turns the corner (corresponding to the closest point between receiver and transmitter) to drive a few meters more distancing the BS again.

The receiving set is modeled in the scenario by means of the radiation pattern of each antenna mounted on the car. They are initially simulated for an empty environment in FEKO. The UWB monopole includes the conical structure, with the hemiellipsoidal dome, and the coaxial feeding. Conducting surfaces are modeled with PEC material and the dielectric of the connector is PTFE (Teflon). On the other hand, the vehicle is modeled with PEC for the body and laminated glass windows, except for the highest frequency. In this case, windows are also conducting to reduce computation time. Wheels and internal elements are excluded to simplify the design and to reduce computational complexity and time consumption during the simulations. Figure 5.2 shows the car model and the four antenna geometries mounted on its roof.

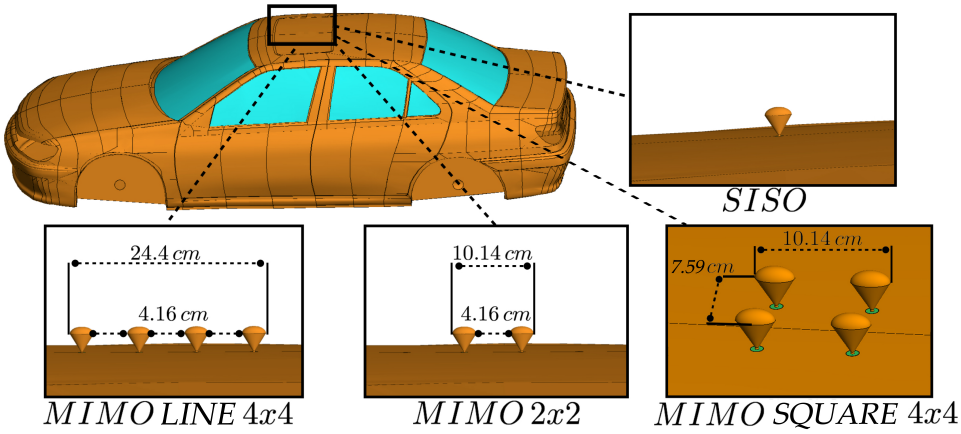

Figure 5.2: Model of the single and multi-antenna geometries mounted on the car.

5.3 V2I Channel Simulation Results

The average capacity for each configuration and frequency is discussed in two different ways. First, the system is assumed to work with a fixed noise level at the receiver. In second term, capacity is compared for different values of Signal to Noise Ratio (SNR), hence, the results are strictly defined by the scattering properties of the channel independently of the power.

5.3.1 Fixed Receiver Noise Level

When the receiver noise is fixed, propagation losses play an important role in capacity. The noise power is estimated to be P_N=-90 dBm, whereas the power transmitted by the BS, P_T, can take different values depending on the particular situation. For BS_{LOS}, P_T is equal to 0 dBm for the two lowest frequencies, i.e, 3.6 and 5.9 GHz, and 10 dBm for 26 GHz. The increment in power is used to partially compensate propagation losses and obtain reasonable values valid for the analysis. Similarly, for BS_{NLOS}, since the direct path is blocked by a building, larger power is used. In particular, P_T is 30 and 40 dBm for lowest and highest bands, respectively.

Each frequency is now analyzed individually to investigate the channel properties at each band. According to the antenna geometry used on the car, the average capacity for the entire trajectory is calculated and compared.

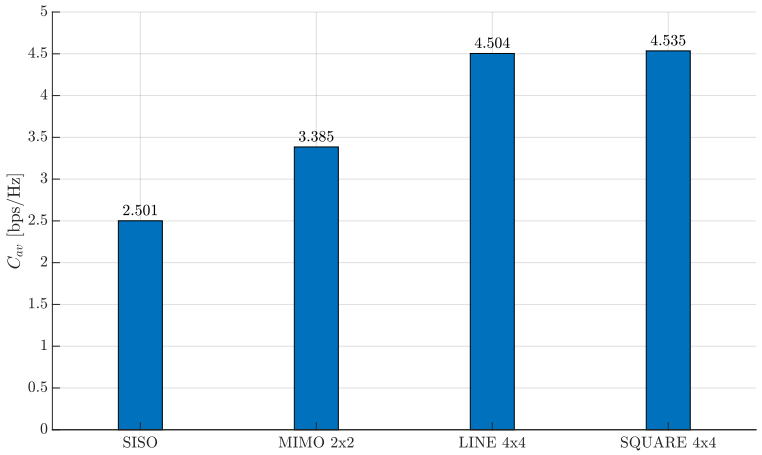

(a) Line of sight.

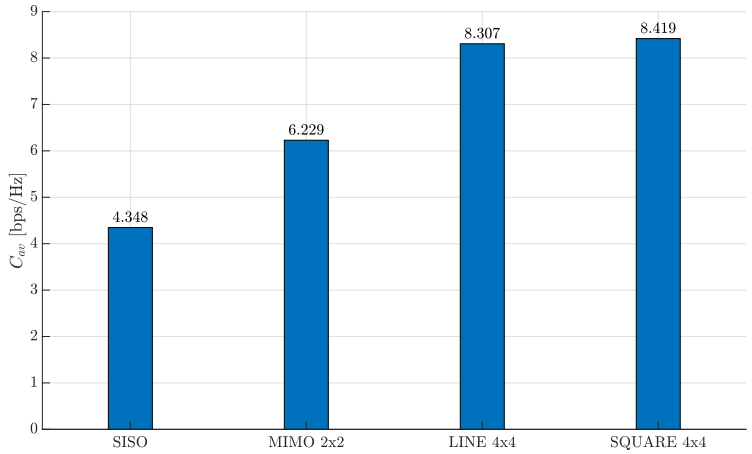

(b) Non line of sight.

Figure 5.3: Average capacity at 3.6 GHz.

The first case is 3.6 GHz. Figure 5.3 shows the average capacity for the two scenarios: LOS (a) and NLOS (b). Looking at the top graph, it is possible to state that capacity is clearly improved using multiple antennas. The gain is 35% for the case of MIMO 2x2 and around 80% for the two 4x4 geometries. This improvement is not only depending on the number of antennas and the correlation between them, but it is also conditioned by the available SNR. In absolute values, the use of a low frequency band implies less propagation losses and, in consequence, higher received power.

The second figure, about NLOS, shows a similar performance, but values are between 73 and 86% larger compared to the LOS. The increment in transmitted power seems to overcompensate the losses due to the direct path blockage. The reflected rays are now much stronger than before and capacity is clearly increased. Regarding the MIMO gain, the use of two antennas implies a gain of 43% and four antennas, over 90%. As previously found in Chapter 4, NLOS situations are richer in terms of scattering but it is only translated into a real improvement in capacity if power loss is somehow compensated. In any case, the use of several radiators improve the achievable rates.

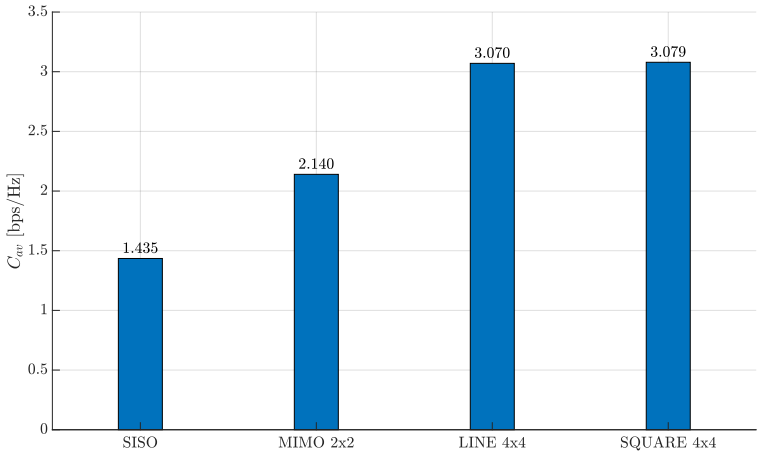

(a) Line of sight.

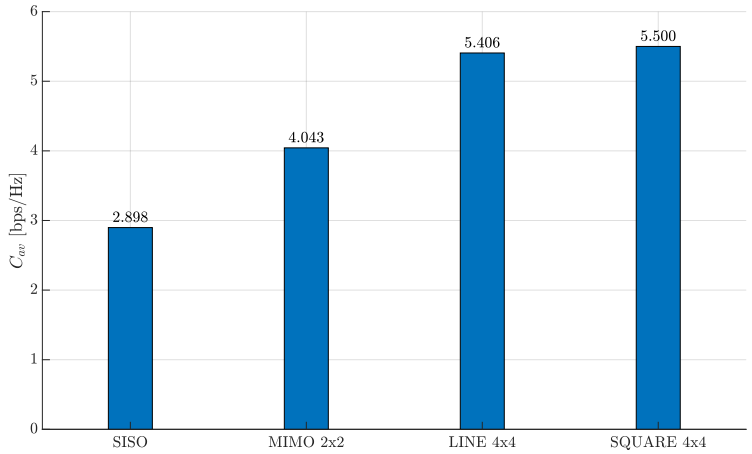

(b) Non line of sight.

Figure 5.4: Average capacity at 5.9 GHz.

Figure 5.4 depicts the average capacity as well, but operating at 5.9 GHz. Values are now smaller than compared to 3.6 GHz, since the received power is smaller. On the other hand, in relative terms, the MIMO gain undergoes different performance depending on the visibility condition. For LOS, the improvement is around 50% when two antennas are used and 114%, for linear and square MIMO 4x4, larger ratios than for the lowest band. By contrast, the NLOS communication suffers a smaller improvement compared to previous case: 40% and 86% for two and four antennas respectively. The best scattering properties at higher frequencies make the system to improve more when there is enough power at the receiver. When the direct path is blocked, the power loss is over the possible improvement on the channel correlation.

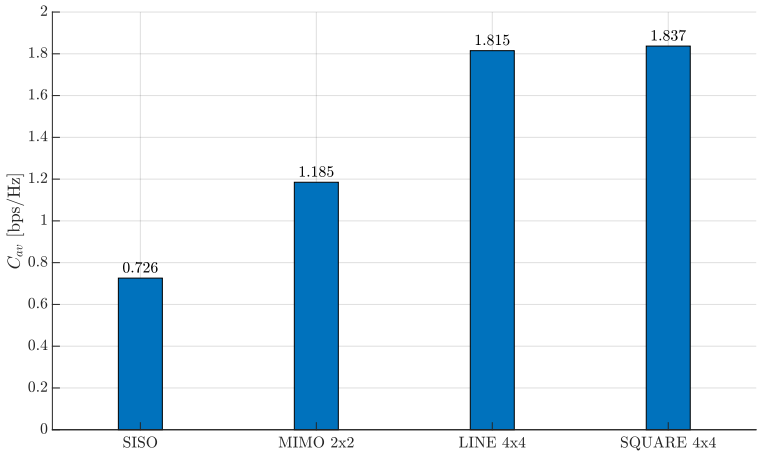

(a) Line of sight.

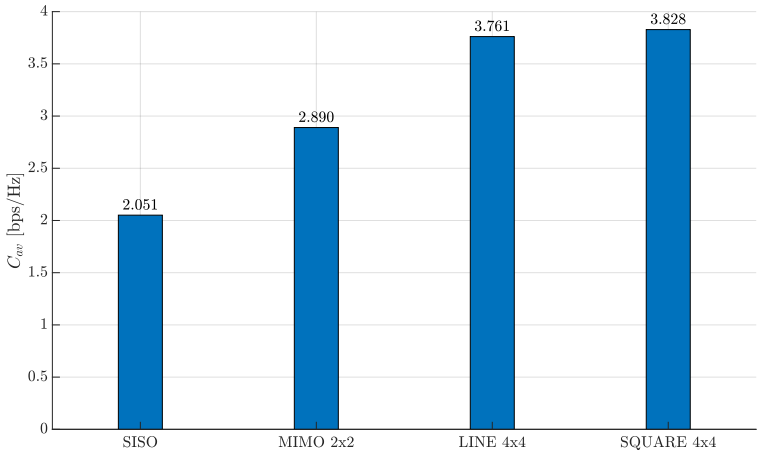

(b) Non line of sight.

Figure 5.5: Average capacity at 26 GHz.

Finally, the 26 GHz band is analyzed. Average capacity is again plotted for the two scenarios in Figure 5.5. The most noticeable change is the high reduction in capacity. Propagation losses are becoming quite restrictive when approaching to mmWave frequencies. In the worst case, when only one antenna is used, less than 1 bps/Hz is obtained for LOS (10 dBm in transmission), but the gain in capacity when MIMO geometries are integrated is larger in comparison to sub-6 GHz bands: 63% for 2x2 and 150% for 4x4. As these values are referenced to SISO, a great improvement is still small in absolute terms, but it demonstrates the good scattering properties at high frequencies. Randomness of reflections is incremented and the channel performs better with several radiators.

Regarding NLOS situation, power is also increased by 30 dB and the resulting values are more than doubled, despite the building not allowing the direct vision. This is the expected behavior when the system is working in a low SNR regime. Due to the logarithmic trace, the increment of capacity with power is larger when signal is low, since the improvement is almost linear. On the other hand, MIMO gain respect to the single antenna is similar to the previous case.

In summary, it has been proven that MIMO improves capacity for scattering rich scenarios, but with some considerations. First, the received power is a critical parameter to decide the order of the multi-antenna geometry. For high frequencies, several antennas help to overcome propagation losses, but a minimum power must be received to ensure a proper communication. In NLOS, doubling the number of elements implies a gain of 40% approximately in capacity. In LOS, the improvement tightly depends on the operating band.

MIMO 4x4 has been analyzed for two different geometries on the car. The obtained values are very similar in all cases, but the capacity associated to the square shape is always slightly above the linear arrangement. Since antennas are always further than a half of the wavelength, increasing the size of the whole geometry does not really improve the performance and it is possible to compact the design in one dimension if antennas are placed in two rows. This may be specially useful for manufacturers to fit their designs into a smaller radome.

5.3.2 MIMO Capacity vs. SNR

The strict relation between power and capacity, as well as the enormous difference in propagation losses between the three bands, make the analysis of the channel scattering properties very complex if same power is assumed. Then, a second study is carried out in which mean SNR along the route is fixed and channel matrices are normalized to be independent from the losses. Therefore, the achievable capacity with equal SNR values only depends on the ray distribution and scattering properties at each operating frequency.

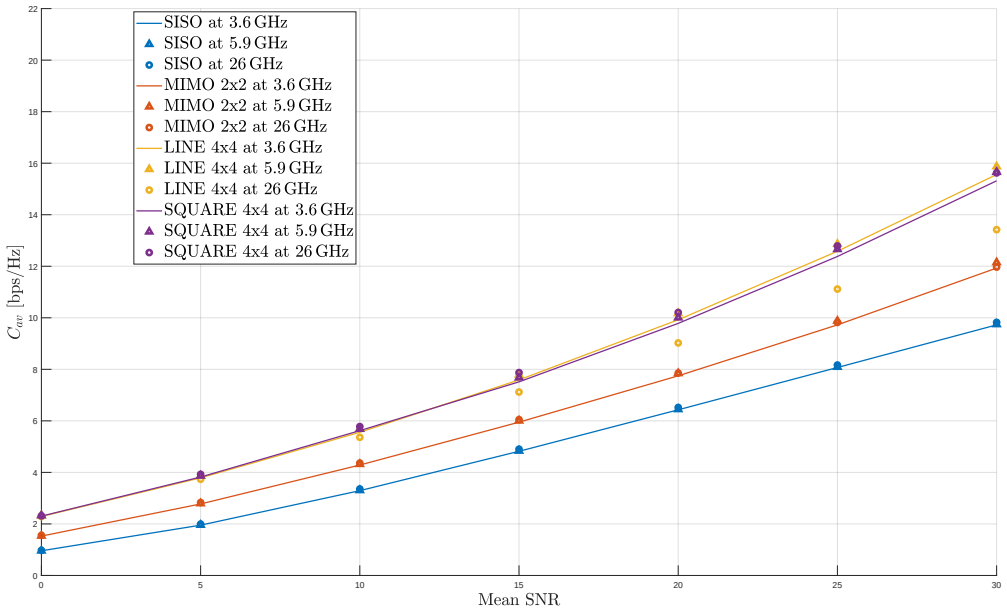

Figure 5.6: Average channel capacity for distinct mean SNR values in the LOS scenario.

The first case to consider is the LOS scenario. Figure 5.6 depicts the average capacity for the three frequencies previously considered and the four geometries on the car as

a function of the mean SNR at the receiver. In general, all lines corresponding to the same number of elements follow a similar trend, except the linear MIMO 4x4 at 26 GHz, which gets closer to the 2x2 lines as the SNR increases. This behavior suggests that, specially for high frequencies, enlarging the geometry in only one dimension is not really improving the capacity. On the other hand, the square modality at high frequencies always performs better than the line.

At second glance, it is possible to notice that the higher the MIMO order, the more pronounced is the slope as the power increases. Due to the logarithmic scale of the x-axis, the SISO traces are following a line, whereas MIMO graphs are almost exponential. This effect is more noticeable as the number of elements is incremented.

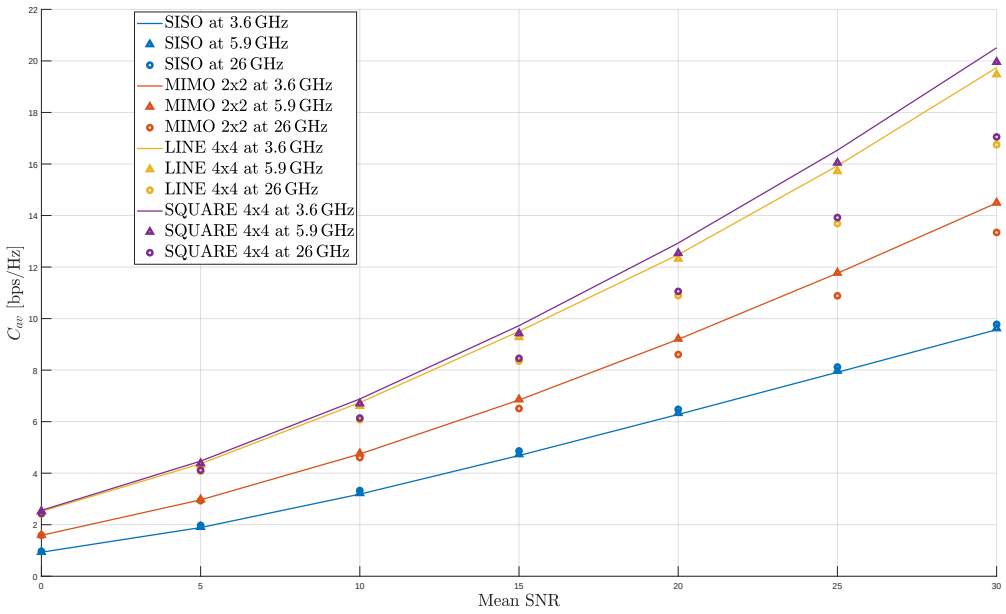

Figure 5.7: Average channel capacity for distinct mean SNR values in the NLOS scenario.

The differences in the channel scattering can be really determined in a NLOS situation, which is shown in Figure 5.7. Contrary to what could be expected, lower frequencies are able to reach higher capacity values, except for single antenna systems, in which all perform in a very similar way. For 26 GHz, it is possible to see a detriment in capacity that can become a 17% in the worst case. This performance is contrary to the previous indoor studies in Chapter 4, in which high frequencies performed better in NLOS. This may be the major difference between indoor and outdoor scenarios. Open environments without direct view tend to benefit lower bands. If the power issue is also considered, due to the frequency-dependant propagation losses, 3.6 GHz seems to be the best choice for large urban scenarios and MIMO geometries can improve substantially the system performance.

Chapter 6

Conclusions

In this thesis, several aspects of next generation mobile communications have been discussed. The main conclusions that can be extracted from the work developed in previous chapters are summarized in the following lines.

It has been demonstrated that all bands of interest below 30 GHz for 5G, LTE and IEEE 802.11 can be covered with one single antenna design. The 3D printing technique allows to create any type of geometry and, by means of the metallizing process, it can be transformed into a radiating element. The potential applications of this procedure extends from prototyping to final and commercial designs if properly implemented. The proposed design, a UWB version of a monopole, is manufactured and tested up to 26 GHz. The results are in good agreement with initial software simulations, which validates the printing and metallizing process.

The antenna is then used for two different applications: an indoor MIMO system and a V2I communication environment. Different multi-antenna geometries are discussed according to the channel performance and achievable capacity.

For both indoor and outdoor V2I cases, it is clearly stated that lower frequencies present better propagation properties. On the other hand, rich environments in terms of scattering are required to take advantage of MIMO and higher frequencies present more and better distributed reflections. A trade-off between power and MIMO gain must be considered.

Regarding the indoor scenario, corresponding to a corridor with a 90 degree corner, it acts as a waveguide for the case of LOS. When the receiver turns the corner and there is no direct vision towards the transmitter, power decreases noticeably. This is specially critical for higher bands. In this case, the use of multiple antennas can overcome the lack of power to improve capacity, but if received signal is too weak, communication may be unfeasible.

A similar analysis can be carried out for the case of the V2I system. NLOS condition benefits the use of several radiators, but it reduces the received power substantially. The main difference respect to the previous case is that vehicle communications are always performed outdoors. The waveguide effect is not present and waves are radiated to the whole space. In this case, the use of sub-6 GHz frequencies is highly recommended.

6.1 Future Work

The work previously presented is just the starting point of a more ambitious project regarding the design of future antenna systems for next-generation networks. In addition, some of the proposals have to be optimized and validated before extending the work to other topics. The indoor measurement campaign is expected to be carried out in short term and some outdoor experiments need to be scheduled as well. The UWB antenna has to be fully tested up to the mmWave band, between 30 and 40 GHz at least. Correlation measurements of multi-antenna geometries are also required to characterize the system.

In a mid- long-term period, there are several proposals to extend this thesis and cover advanced topics of 5G networks. The consideration of massive antennas is mandatory to improve the efficiency and introduce spatial multiplexing techniques, which seem to be crucial in future systems. It also leads to larger bandwidths and higher frequencies in the mmWave region. 60 GHz is a promising candidate for many applications, since the unlicensed usage is allowed.

The use of optical systems to create signals in the millimetric or terahertz region is another scope of research. It allows the efficient transport of signals through fiber and bandwidth is not a real limitation. The management of several users and the design of appropriate antennas are the most important challenges in this direction.

In conclusion, the close horizon of the next mobile generation is speeding up antenna designers to provide innovative and feasible solutions to create a new era of efficient, green, ultra-fast and massively deployed networks. This thesis tried to cover some aspects and introduce others for future research lines.

6.2 Research Outcome

The following articles have been published or submitted as a consequence of the work presented in this thesis and closely related topics:

- C. Ballesteros, A. Pfadler, J. Romeu, L. Jofre, "5G Vehicle MIMO Antenna Capacity Based on a Rigorous Electromagnetic Channel Modeling", 2018 48th European Microwave Conference (EuMC), Madrid, September 2018.
- A. Pfadler, C. Ballesteros, J. Romeu and L. Jofre, "Multi-antenna Configuration Modeling for Massive MIMO V2I", 12th European Conference on Antennas and Propagation (EuCAP), London, April 2018.
- A. Pfadler, C. Ballesteros, J. Romeu and L. Jofre, "Vehicle Antenna Footprint Optimization for Efficient MIMO V2X Communications", 10th International Conference on Adaptive and Self-Adaptive Systems and Applications (ADAPTIVE), Barcelona, February 2018.
- C. Ballesteros, A. Pfadler, L. Jofre and J. Romeu, "Antenna Geometry Optimization for MIMO Connected Cars", XXXII URSI National Symposium, Cartagena, September 2017.

- A. Pfadler, C. Ballesteros, J. Romeu and L. Jofre, "Propagation-Based Performance of Massive MIMO Antenna Configurations for V2I Urban Communications", Special Issue on Radio Wave Propagation, IEEE Transaction on Antennas and Propagation, Under Revision.

Bibliography

[1] A. Pfadler, C. Ballesteros, J. Romeu, and L. Jofre, "Multi-antenna Configuration Modeling for Massive MIMO V2I," in *12th European Conference on Antennas and Propagation (EuCAP)*, EurAPP, 2018.

[2] A. Pfadler, C. Ballesteros, J. Romeu, and L. Jofre, "Vehicle Antenna Footprint Optimization for Efficient MIMO V2X Communications," in *10th International Conference on Adaptive and Self-adaptive Systems and Applications (ADAPTIVE)*, IARIA, 2018.

[3] The 5G Infrastructure Public Private Partnership, "5G-PPP." [Online]. Available: `https://5g-ppp.eu` [Accessed: 2018-04-02].

[4] European Comission, "Horizon 2020: Work Programme 2018-2020," Jan. 2018.

[5] Rysavy Research for 4G Americas, "Mobile Broadband Explosion: The 3GPP Wireless Evolution." White Paper, Aug. 2013.

[6] P. Bergadà *et al.*, "Digital transmission techniques for a long haul HF link: DSSS versus OFDM," *Radio Sci.*, vol. 49, pp. 518–530, July 2014.

[7] Alan Weissberger, "ITU-R agrees on key performance requirements for IMT-2020="5G"." IEEE Communications Society. Technology Blog [Online], Mar. 2017. Available: `http://techblog.comsoc.org/2017/03/02/itu-r-agrees-on-key-performance-requirements-for-imt-20205g/` [Accessed: 2018-04-02].

[8] S. Kutty and D. Sen, "Beamforming for millimeter wave communications: An inclusive survey," *IEEE Communications Surveys Tutorials*, vol. 18, pp. 949–973, Secondquarter 2016.

[9] B. Ai, K. Guan, M. Rupp, T. Kurner, X. Cheng, X. F. Yin, Q. Wang, G. Y. Ma, Y. Li, L. Xiong, and J. W. Ding, "Future railway services-oriented mobile communications network," *IEEE Communications Magazine*, vol. 53, pp. 78–85, October 2015.

[10] J. Li, B. Ai, R. He, M. Yang, Q. Wang, B. Zhang, and Z. Zhong, "Cluster-based 3-d channel modeling for massive mimo in subway station environment," *IEEE Access*, vol. 6, pp. 6257–6272, 2018.

[11] I. N. S. Academy, *Pursuit and Promotion of Science: The Indian Experience*. Indian National Science Academy, 2001.

[12] A. K. Sen, "Sir j.c. bose and millimeter waves," in *TENCON '98. 1998 IEEE Region 10 International Conference on Global Connectivity in Energy, Computer, Communication and Control*, vol. 2, pp. 288–290 vol.2, 1998.

[13] D. T. Emerson, "The work of jagadis chandra bose: 100 years of mm-wave research," in *International Microwave Symposium Digest*, vol. 2, pp. 553–556, IEEE MTT-S, 1997.

[14] E. Nichols and J. Tear, "Short electric waves," *Physical Review*, vol. 21, no. 6, p. 587, 1923.

[15] J. Tear, "The optical constants of certain liquids for short electric waves," *Physical Review*, vol. 21, no. 6, p. 611, 1923.

[16] C. E. Cleeton and N. H. Williams, "Electromagnetic waves of 1.1 cm wave-length and the absorption spectrum of ammonia," *Physical Review*, vol. 45, no. 4, p. 234, 1934.

[17] J. Dees, J. King, and J. Wiltse, "A millimeter wave propagation experiment from the ats-e spacecraft," *Technical Report*, 1968.

[18] P. Curtis, G. Peskett, and C. Rodgers, "Remote sounding of atmospheric temperature from satellites v. the pressure modulator radiometer for nimbus f," *Proc. R. Soc. Lond. A*, vol. 337, no. 1608, pp. 135–150, 1974.

[19] J. C. Wiltse, "History of millimeter and submillimeter waves," *IEEE Transactions on Microwave Theory and Techniques*, vol. 32, pp. 1118–1127, Sep 1984.

[20] Y. J. Kim, L. Jofre, F. D. Flaviis, and M. Q. Feng, "Microwave reflection tomographic array for damage detection of civil structures," *IEEE Transactions on Antennas and Propagation*, vol. 51, pp. 3022–3032, Nov 2003.

[21] L. Jofre, A. Broquetas, J. Romeu, S. Blanch, A. P. Toda, X. Fabregas, and A. Cardama, "Uwb tomographic radar imaging of penetrable and impenetrable objects," *Proceedings of the IEEE*, vol. 97, pp. 451–464, Feb 2009.

[22] L. Yujiri, M. Shoucri, and P. Moffa, "Passive millimeter wave imaging," *IEEE Microwave Magazine*, vol. 4, pp. 39–50, Sept 2003.

[23] D. M. Sheen, D. L. McMakin, and T. E. Hall, "Three-dimensional millimeter-wave imaging for concealed weapon detection," *IEEE Transactions on Microwave Theory and Techniques*, vol. 49, pp. 1581–1592, Sep 2001.

[24] E. S. Rosenblum, *Atmospheric Absorption of 10-400 KMcps Radiation: Summary and Bibliography to 1960.* Massachusetts Institute of Technology, Lincoln Laboratory, 1960.

[25] H. T. Friis, "A note on a simple transmission formula," *Proceedings of the IRE*, vol. 34, pp. 254–256, May 1946.

[26] Int Telecom Union - Radiocom Sector (ITU-R), *Final Acts - World Radiocommunication Conference (WRC-15)*, Nov. 2015.

[27] A. Morgado, K. M. S. Huq, S. Mumtaz, and J. Rodriguez, "A survey of 5g technologies: regulatory, standardization and industrial perspectives," *Digital Communications and Networks*, vol. 4, no. 2, pp. 87 – 97, 2018.

[28] The 3rd Generation Partnership Project (3GPP), "Release 15." [Online]. Available: http://www.3gpp.org/release-15 [Accessed: 2018-05-02].

[29] The 3rd Generation Partnership Project (3GPP), "First 5G NR Specs Approved." [Online]. Available: http://www.3gpp.org/news-events/3gpp-news/1929-nsa_nr_5g [Accessed: 2018-05-02].

[30] Qualcomm Technologies, Inc., "Making 5G NR a reality." [Online]. Available: https://www.qualcomm.com/documents/making-5g-nr-reality [Accessed: 2018-06-20].

[31] GlobalFoundries, Inc., "Design Innovations in 5G mmWave FEMs and Phased Arrays." [Online]. Available: https://www.globalfoundries.com/resources/technical-webinar-series/design-innovations-5g-mmwave-fems-and-phased-arrays [Accessed: 2018-03-14].

[32] Car 2 Car Communication Consortium (C2C-CC), "Position Paper: Frequency Bands for V2X," Jan. 2017.

[33] 5G Americas, "Cellular V2X Communications towards 5G," Mar. 2018.

[34] "Access layer specification for Intelligent Transport Systems operating in the 5 GHz frequency band," *ETSI EN 302 663 V.1.2.0*, Nov. 2012.

[35] "Part 11: Wireless LAN Medium Access Control (MAC) and Physical Layer (PHY) Specifications," *IEEE Standard 802.11p 2010*, July 2010.

[36] Q. X. Chu and Y. Y. Yang, "A compact ultrawideband antenna with 3.4/5.5 ghz dual band-notched characteristics," *IEEE Transactions on Antennas and Propagation*, vol. 56, pp. 3637–3644, Dec 2008.

[37] Ultra-Wideband Operation FCC, "Report and order," *In the matter of Revision of Part l5 the Commission's Rules Regarding Ultra-Wideband Transmission Systems*, vol. 21, 2002.

[38] M. Ito, "Dispersion of very short microwave pulses in waveguide," *IEEE Transactions on Microwave Theory and Techniques*, vol. 13, pp. 357–364, May 1965.

[39] W. S. Yeoh and W. S. T. Rowe, "An UWB conical monopole antenna for multi-service wireless applications," *IEEE Antennas and Wireless Propagation Letters*, vol. 14, pp. 1085–1088, 2015.

[40] G. Santra and B. Ghosh, "A coaxial fed solid half conical monopole antenna for multiple wireless and satellite communications," in *2016 International Conference on Radar, Antenna, Microwave, Electronics, and Telecommunications (ICRAMET)*, pp. 103–105, Oct 2016.

[41] S. Ramanujan, "Modular equations and approximations to π," *Quart. J. Math*, vol. 45, pp. 350–372, 1914.

[42] C. H. Papas and R. King, "Input impedance of wide-angle conical antennas fed by a coaxial line," *Proceedings of the IRE*, vol. 37, pp. 1269–1271, Nov 1949.

[43] Altair Hyperworks, *FEKO User Manual 2017.2*. Altair Engineering Inc., 2017.

[44] Altair Engineering, Inc., "FEKO." [Online]. Available: `https://altairhyperworks.com/product/FEKO` [Accessed: 2018-04-30].

[45] Huber + Suhner AG, *23_SMA-50-0-3/111_NE Datasheet*.

[46] Y. Park and H. Kim, "On the coexistence of ieee 802.11ac and wave in the 5.9 ghz band," *IEEE Communications Magazine*, vol. 52, pp. 162–168, June 2014.

[47] G. Spencer and M. Murty, "General ray-tracing procedure," *JOSA*, vol. 52, no. 6, pp. 672–678, 1962.

[48] Z. Yun and M. F. Iskander, "Ray tracing for radio propagation modeling: Principles and applications," *IEEE Access*, vol. 3, pp. 1089–1100, 2015.

[49] R. H. Clarke, "A statistical theory of mobile-radio reception," *The Bell System Technical Journal*, vol. 47, pp. 957–1000, July 1968.

[50] S. Blanch, J. Romeu, and I. Corbella, "Exact representation of antenna system diversity performance from input parameter description," *Electronics Letters*, vol. 39, pp. 705–707, May 2003.

[51] G. J. Foschini and M. J. Gans, "On limits of wireless communications in a fading environment when using multiple antennas," *Wireless personal communications*, vol. 6, no. 3, pp. 311–335, 1998.

[52] C.-N. Chuah, D. N. C. Tse, J. M. Kahn, and R. A. Valenzuela, "Capacity scaling in mimo wireless systems under correlated fading," *IEEE Transactions on Information Theory*, vol. 48, pp. 637–650, Mar 2002.